© 2015. Published by The Company of Biologists Ltd | Development (2015) 142, 2452-2463 doi:10.1242/dev.125492

RESEARCH ARTICLE

The intracellular domains of Notch1 and Notch2 are functionally equivalent during development and carcinogenesis

Zhenyi Liu[1], Eric Brunskill[2], Barbara Varnum-Finney[3], Chi Zhang[4], Andrew Zhang[5], Patrick Y. Jay[6], Irv Bernstein[3,7], Mitsuru Morimoto[8] and Raphael Kopan[2,*]

ABSTRACT

Although Notch1 and Notch2 are closely related paralogs and function through the same canonical signaling pathway, they contribute to different outcomes in some cell and disease contexts. To understand the basis for these differences, we examined in detail mice in which the Notch intracellular domains (N1ICD and N2ICD) were swapped. Our data indicate that strength (defined here as the ultimate number of intracellular domain molecules reaching the nucleus, integrating ligand-mediated release and nuclear translocation) and duration (half-life of NICD-RBPjk-MAML-DNA complexes, integrating cooperativity and stability dependent on shared sequence elements) are the factors that underlie many of the differences between Notch1 and Notch2 in all the contexts we examined, including T-cell development, skin differentiation and carcinogenesis, the inner ear, the lung and the retina. We were able to show that phenotypes in the heart, endothelium, and marginal zone B cells are attributed to haploinsufficiency but not to intracellular domain composition. Tissue-specific differences in NICD stability were most likely caused by alternative scissile bond choices by tissue-specific γ-secretase complexes following the intracellular domain swap. Reinterpretation of clinical findings based on our analyses suggests that differences in outcome segregating with Notch1 or Notch2 are likely to reflect outcomes dependent on the overall strength of Notch signals.

KEY WORDS: Notch, Domain swap, Endothelium, Heart, Marginal zone B cells, Carcinogenesis

INTRODUCTION

The Notch signaling pathway is active in all metazoa, with a single receptor present in *Drosophila*, two in *Caenorhabditis elegans* and four in mammals (Kopan and Ilagan, 2009). Multiple lines of evidence suggest that the two most related mammalian Notch paralogs (Notch1 and Notch2) have different, and at times opposite, biological functions, most notably in predicting survival of cancer patients (Boulay et al., 2007; Chu et al., 2011; Fan et al., 2004; Graziani et al., 2008; Parr et al., 2004). This latter observation presents an interesting challenge therapeutically, the resolution of which requires a mechanistic framework that can explain this apparent divergence in function between Notch1 and Notch2.

Notch proteins are large transmembrane receptors that become activated by transmembrane ligands of the Delta/Serrate/Lag-2 (DSL) family [reviewed by Kopan and Ilagan (2009)]. Ligand binding unfolds a protective juxtamembrane domain (Kovall and Blacklow, 2010) to expose the protein to ADAM10 cleavage (Groot et al., 2013; van Tetering et al., 2009). The remaining peptide undergoes cleavage by the γ-secretase complex (Jorissen and De Strooper, 2010), releasing the Notch intracellular domain (NICD). NICD stability is determined by the identity of the amino terminal amino acid (Blat et al., 2002) and by a degron(s) that is phosphorylated after assembly of a transcription complex (Chiang et al., 2006; Fryer et al., 2004). In considering how Notch1 and Notch2 proteins could contribute differentially to disease outcome, the simplest model suggests differential NICD composition. This model assumes that the evolution of N1ICD and N2ICD resulted in preferred association with other cellular proteins or transcription factors, which would modify the outcome differentially.

Motivated by these observations and by the apparent asymmetric functions of Notch1 and Notch2 in renal development (Cheng et al., 2007), we created two new strains of mice harboring rearranged *Notch1* and *Notch2* loci (Liu et al., 2013): *Notch12* (N12) and *Notch21* (N21). In response to ligands, the *Notch1* extracellular and transmembrane domain of the N12 allele is sequentially cleaved to release the *Notch2* ICD (N2ICD; Fig. 1A,B); reciprocally, cleavage of the *Notch2* extracellular and transmembrane domain of the N21 allele releases the *Notch1* ICD (N1ICD; Fig. 1A,B) (Liu et al., 2013). Using these strains, we analyzed kidney development and found no support for the hypothesis that NICD composition was driving the differences between the two receptors. Instead, we identified a different mechanism that explained the divergent function of Notch1 and Notch2 in kidney development (Liu et al., 2013). We discovered that in the kidney Notch2 constituted the larger proportion of Notch receptors at the cell surface and was cleaved in response to ligands more efficiently, and that these differences were coded by the amino acid composition of the extracellular domain (ECD). N1ICD and N2ICD were perfectly equivalent: 100% of nephrons were rescued by the N1ICD when it was expressed from the *Notch2* locus, whereas no nephron formed when N2ICD was solely produced from the *Notch1* locus (in *Pax3-Cre, N2$^{f/f}$, N1$^{12/12}$* animals, which lack endogenous Notch2 in the developing kidney; see figure 3 of Liu et al., 2013). This mirrors the absolute requirement for Notch2 in kidney development (Cheng et al., 2007). The importance of the ECD in transporting Notch and ensuring cleavage efficiency *in vivo* was confirmed recently by comparing N1 and NIP1::Cre proteolysis (Liu et al., 2015).

As conclusive and unequivocal as these results are, they did not rule out the possibility that NICD composition does play a role in other

[1]SAGE Labs, A Horizon Discovery Group Company, St Louis, MO 63146, USA. [2]Division of Developmental Biology, Children's Hospital Medical Center, Cincinnati, OH 45229, USA. [3]Clinical Research Division, Fred Hutchinson Cancer Research Center, Seattle, WA 98109, USA. [4]Department of Clinical Medicine, University of Oxford, Oxford OX3 7BN, UK. [5]University of Minnesota Medical School, Minneapolis, MN 55455, USA. [6]Departments of Pediatrics and Genetics, Washington University, St Louis, MO 63110, USA. [7]Department of Pediatrics, University of Washington, Seattle, WA 98195, USA. [8]Lung Development and Regeneration, RIKEN Center for Developmental Biology, Kobe 650-0047, Japan.

*Author for correspondence (Raphael.kopan@cchmc.org)

Received 17 April 2015; Accepted 2 June 2015

Development (2015) 142, 2452-2463 doi:10.1242/dev.125492

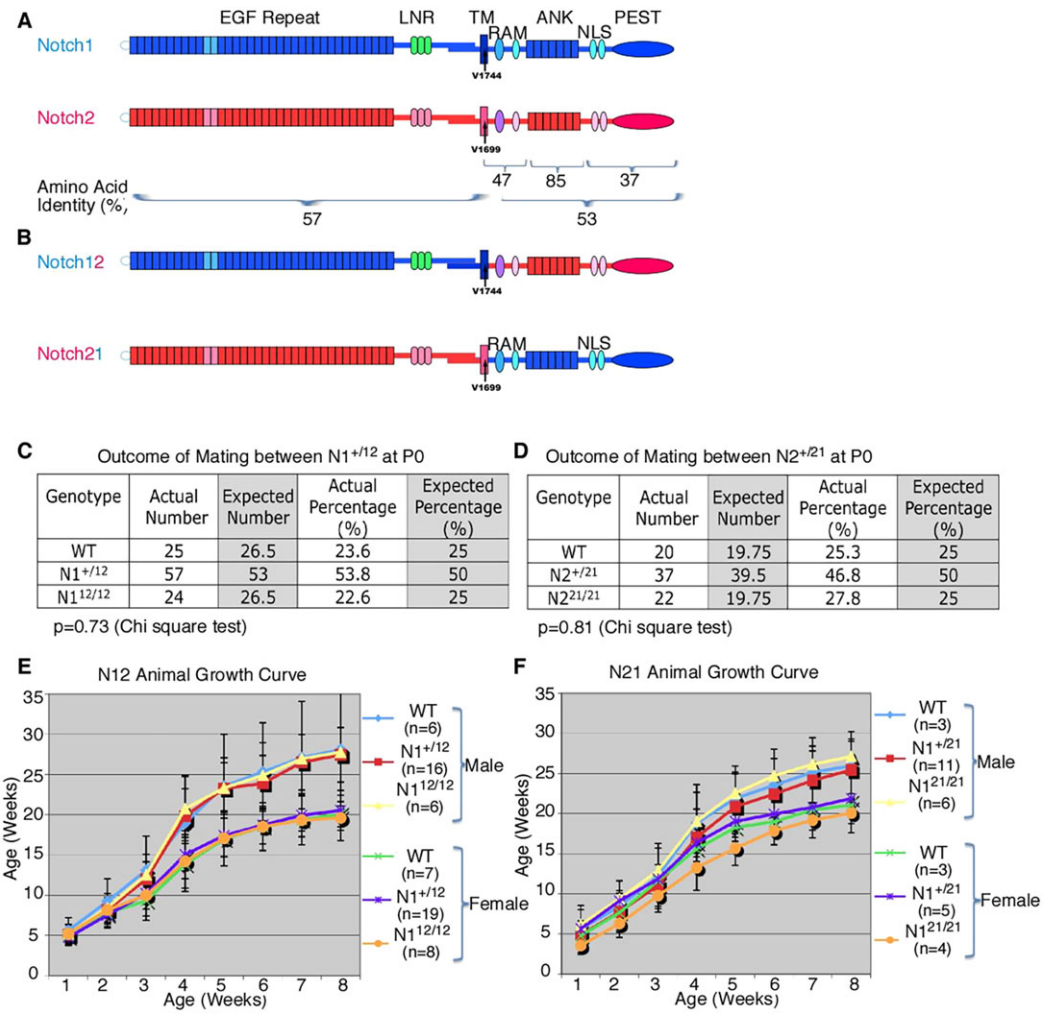

Fig. 1. Swap of the intracellular domains of Notch1 and Notch2 did not affect animal survival and growth on mixed background. (A,B) Domain structure of wild-type Notch1 and Notch2 (A) and chimeric Notch12 and Notch21 (B) proteins. ANK, ankyrin repeats; EGF repeat, epidermal growth factor repeat; LNR, Lin-Notch repeat; NLS, nuclear localization signal; PEST, proline/glutamic acid/serine/threonine-rich motifs; RAM, RBPjk association module; TM, transmembrane domain. (C,D) Homozygote $N1^{12/12}$ (C) and $N2^{21/21}$ (D) were born at expected Mendelian ratios. (E,F) The growth rates of homozygote $N1^{12/12}$ (E) and $N2^{21/21}$ (F) are similar to those of their sex-matched littermates. Error bars represent s.d.

tissues. To address this possibility, we analyzed a multitude of cell types and organs in the N12 and N21 strains with special attention given to those in which either Notch1 or Notch2 plays dominant roles, reasoning that this could reflect nuclei where NICD composition plays an important role. We also examined the role of NICD composition in skin carcinogenesis. Overall, we still could not demonstrate one case in which composition played a significant role. Instead, we uncovered multiple lines of evidence indicating that the Notch signaling pathway is exquisitely sensitive to NICD dosage. The significance of these data to disease outcome will be discussed.

RESULTS

Outbred N12 and N21 homozygous mice display no overt phenotype

We have analyzed the N12 and N21 strains of mice for overall morphological and growth parameters. When the lines were maintained on a mixed genetic background, both N12/12 and N21/21 homozygous pups were born at the expected Mendelian frequencies (Fig. 1C,D), despite the presence of Notch receptors releasing exclusively N1ICD ($N1^{+/+}$; $N2^{21/21}$) or N2ICD ($N1^{12/12}$; $N2^{+/+}$). Because delta-like 1 (*Dll1*) haploinsufficiency affects metabolic pathways and growth (Rubio-Aliaga et al., 2009, 2007), we wondered whether the monotone composition of NICD in N21 and N12 homozygote animals would result in similar deficiencies. We monitored weight gain as a surrogate for metabolic state over an eight-week period after birth and concluded that these mice were indistinguishable from gender-matched wild-type littermates in their growth rates (Fig. 1E,F).

Some organs in which either Notch1 or Notch2 are dominant develop normally

We have recently shown that the cell surface distribution and the efficiency of activation upon ligand binding, but not NICD composition, resulted in a dominant contribution of Notch2 to kidney development (Liu et al., 2013). To extend this analysis to other organs in which one receptor is acting alone or is dominant over its paralog, we examined the development of T cells (Fiorini et al., 2009), the inner ear (Kiernan et al., 2005; Zhang et al., 2000), the endocardium (MacGrogan et al., 2010) and skin (Demehri et al., 2008; Rangarajan et al., 2001), where *Notch1* is dominant, and the liver (Geisler et al., 2008), eye (Geisler et al., 2008; McCright et al., 2002), cardiac neural crest cells (McCright

Development (2015) 142, 2452-2463 doi:10.1242/dev.125492

et al., 2001; Varadkar et al., 2008) and lung (Morimoto et al., 2012), where *Notch2* is dominant. Analysis of hair cell distribution within the cochlea of N12 homozygote mice demonstrated the same infrequent perturbations in patterning as seen in their wild-type littermates (Fig. 2A-C). In *Notch1*-deficient animals, a block in T-cell development manifests by accumulation of double negative CD4/CD8 cells (DN cells) with DN1 characteristics (Radtke et al., 1999), demonstrating an essential role for Notch1 in T-cell development and lineage commitment in the thymus. We detected similar proportions of DN, double- and single-positive CD4/CD8 T cells in the thymus of N12 homozygous and wild-type mice (Fig. 2D). A more detailed analysis of DN subtypes confirmed a normal transition through the *Notch1*-dependent DN1-DN3 gate (Fig. 2E). Together, these observations establish that the amino acid composition of N2ICD conserved all the key residues necessary for full function in organs that develop only in the presence of N1ICD. A similar conclusion emerged in five *Notch2*-dependent organs: the kidney (Liu et al., 2013), the lung (Fig. 2F), the liver, the eye and the heart (Fig. 2G).

Whereas the N2ICD could provide all the necessary functions for proper T-cell development in the thymus of $N1^{12/12}$ mice, it is possible that N1ICD could induce ectopic T-cell development from common lymphoid progenitors (CLPs) in the bone marrow (BM) of $N2^{21/21}$ mice, where normally only B cells develop and *Notch2* is expressed in a Jag1-dominated environment (Stanley and Guidos, 2009). We therefore analyzed BM cells for the presence of ectopic T cells by examining the surface marker CD4, CD8, CD44 and CD25 signatures and uncovered no evidence for ectopic T-cell development in the BM, indicating no effect of swapped ICD on promotion of early T-cell differentiation (data not shown). To extend the analysis and examine the impact of specific ligands, we used an *in vitro* system to titrate Notch signal strength as described previously (Dallas et al., 2005; Varnum-Finney et al., 2011). No significant differences were seen in the ability of wild-type and $N2^{21/21}$ hematopoietic stem cells (HSCs) to generate SK^+CD11b^- progenitors or $CD25^+$ (DN2 cells) at any ligand concentration (supplementary material Fig. S1). Combined, these analyses established that ICD1 was equivalent to ICD2 for inducing self-renewal of SK^+ cells and inhibiting myeloid

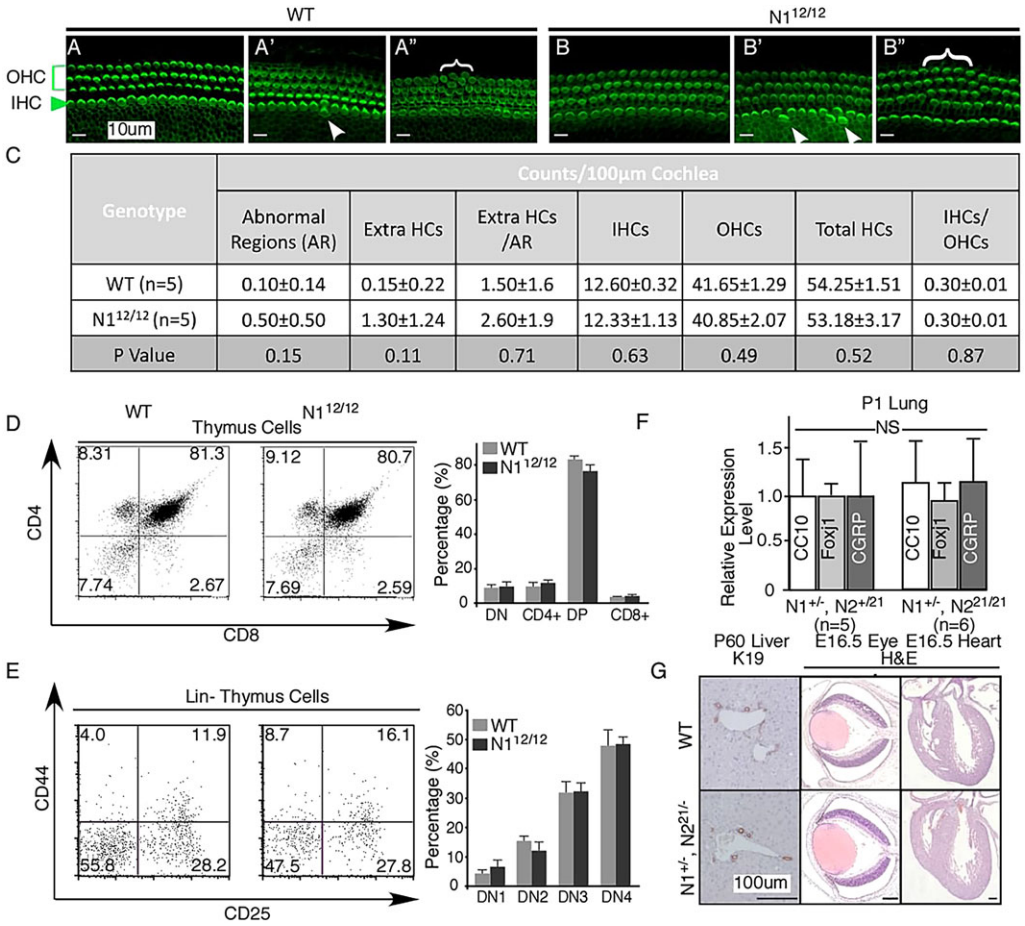

Fig. 2. Swap of the intracellular domains of Notch1 and Notch2 did not have a significant effect on the development of major organs in which either Notch1 (inner ear, T cells) or Notch2 (lung, liver and eye) have dominant roles. (A-C) The inner ear of $N1^{12/12}$ homozygotes (B-B″) has slightly more abnormal regions and extra hair cells compared with their wild-type littermates (A,C), but this is not statistically significant (C). Hair cells are stained with FITC-conjugated phalloidin. OHC, outer hair cells; IHC, inner hair cells. Arrowheads point to single extra hair cells and brackets indicate multiple extra hair cells. (D,E). $N1^{12/12}$ homozygote animals have similar distributions of $CD4^+$, $CD8^+$, $CD4^+CD8^+$, $CD4^-CD8^-$ cells (D) and $CD25^+$, $CD44^+$, $CD25^+CD44^+$, $CD25^-CD44^-$ cells (E). (F) qRT-PCR analysis of different lineage marker expression in newborn lung of $N1^{+/-}$, $N2^{+/21}$ and $N1^{+/-}$, $N2^{21/21}$ show no differences. NS, not statistically significant. CC10, marker for Clara cells; Foxj1, marker for ciliated cells; CGRP, marker for pulmonary neuroendocrine cells. (G) No obvious difference could be detected in the liver of $N1^{+/-}$, $N2^{21/-}$ animals after staining with Keratin 19, a bile duct epithelial cell marker; similarly, no morphological abnormality could be detected in the eye and heart of these animals after H&E staining. Error bars represent s.d.

Development (2015) 142, 2452-2463 doi:10.1242/dev.125492

differentiation *in vivo* and *in vitro*, which we have previously shown is dependent on Notch2 (Varnum-Finney et al., 2011). Thus, amino acids unique to N1ICD were not selected to favor cooperative interactions with T cell-specific inducers.

Disruption of skin barrier function results in the production of thymic stromal lymphopoietin (TSLP), which in turn leads to a dramatic expansion in B-cell proliferation during the first three weeks of life (Demehri et al., 2008). To define further the role of NICD in skin homeostasis, we took advantage of the availability of antibodies specific to Notch1 and Notch2 (characterized in Liu et al., 2013). Careful examination of *Notch1* and *Notch3* expression during development revealed expression in the ectoderm prior to stratification. Expression in the basal layer was expanded into the supra basal layers after epidermal stratification (Fig. 3; supplementary material Fig. S2). By contrast, *Notch2* was only detected in supra-basal cells (Fig. 3; supplementary material Fig. S2). This distribution suggested that a dominant role for *Notch1* in skin development (Demehri et al., 2008; Pan et al., 2004) and homeostasis (Demehri et al., 2009) reflected its function in the basal cell population (Tadeu and Horsley, 2013). To test whether N1ICD composition has any unique function in the skin, we examined the levels of the cytokine TSLP and performed a complete blood count (CBC) in the serum of animals with various combinations of *Notch1* and *Notch2* alleles (Fig. 4A,B). The presence of one N12 allele (Fig. 4Ad,Bd) was sufficient to maintain normal skin differentiation as judged by TSLP levels and white blood cell (WBC) counts, even in the absence of *Notch2* (Fig. 4Af). We noted, however, that in this sensitized background the N2ICD protein was not as potent as N1ICD and a very weak hair phenotype was noticeable along the dorsal midline (Fig. 4Be, *Msx2cre; N1$^{+/f}$; N2$^{f/f}$* versus Fig. 4Bf, *Msx2cre; N1$^{12/f}$; N2$^{f/f}$*). Conversely, restoring the expression of N1ICD from the *Notch2* locus in animals lacking *Notch1* (Fig. 4Ah,Bh, *Msx2cre; N1$^{f/f}$; N2$^{+/21}$*; Fig. 4Ai,Bi, *Msx2cre; N1$^{f/f}$; N2$^{21/21}$*; Fig. 4Ak,Bk, *Msx2cre; N1$^{f/f}$; N2$^{21/f}$*) provided no relief as judged by TSLP levels, WBC counts and skin pathology (supplementary material Fig. S3, compare the K14 staining pattern among *Msx2cre; N1$^{f/f}$; N2$^{21/21}$* and *Msx2cre; N1$^{f/f}$* and *Msx2cre; N2$^{f/f}$*).

A slight difference in activity might be amplified in a chemical carcinogenesis assay (Demehri et al., 2009). To test this possibility, we compared tumor latency and tumor burden in mice lacking *Notch1* but with wild-type (*Msx2cre; N1$^{f/f}$; N2$^{+/+}$*) or N21 proteins expressed at the *Notch2* locus (*Msx2cre; N1$^{f/f}$; N2$^{+/21}$*) (Fig. 4C-E; supplementary material Fig. S3). We observed no differences in the time to tumor formation and all animals developed at least one tumor. However, we noted a significant difference in the number of tumors that developed by week 25 post-7,12-dimethylbenz[a] anthracene (DMBA) treatments. Instead of protecting from chemical carcinogens, the N21 allele seems to be slightly weaker than the wild-type allele. Because N12 and N21 were created in B6 embryonic stem cell lines, this difference was not attributable to strain contributions (Quigley et al., 2009). Combined, this report and the results in Fig. 4Bf,E suggested that ICD composition was not likely to be important.

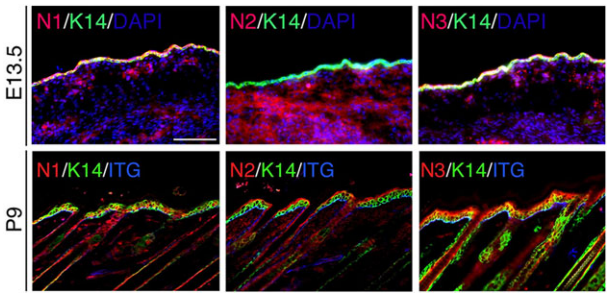

Fig. 3. The expression pattern of Notch paralogs in the epidermis of E13.5 and postnatal day (P) 9 wild-type mice. K14 (Keratin 14) marks the basal cell layer and ITG (Integrin subunit β1) marks the basal membrane of the basal cell layer.

We next tested the possibility that the N12 and N21 alleles differ slightly in their stability due to the selection of cleavage sites by γ-secretase, which can be affected by the composition of charged amino acids near the transmembrane domain (Tagami et al., 2008). In turn, shifting cleavage sites will alter the identity of the amino-terminal residue, affecting stability of some NICD species (Blat et al., 2002). To examine this possibility, we compared the amount of N2ICD released from N12 alleles in N1$^{12/12}$ homozygotes with that of N1ICD released from N1 alleles in wild type (N1$^{+/+}$) in various organs, including the kidney, brain, heart and epidermis, in newborn pups (Fig. 5). This is possible because N2ICD released from N12 protein and N1ICD that are released from N1 protein share the same six N-terminal amino acids and therefore can be recognized by the anti-cleaved Notch1 V1744 antibody with equal affinity (see supplementary material Fig. S4D). We noted differences in the reactive amount of the V1744 antigen in these tissues between wild-type and N1$^{12/12}$ mice, with the epidermis containing the least relative amount of V1744 antigen in N1$^{12/12}$ mice. This result could imply that the selection of S3 cleavage sites varied from tissue to tissue in accordance with tissue-specific composition of γ-secretase (Jorissen and De Strooper, 2010). To access the overall amounts of NICD, we analyzed C-terminal-tagged N1 and N12 in HEK293 cells (supplementary material Fig. S4). The identity of the band containing the NICD was confirmed by its sensitivity to DAPT, a γ-secretase inhibitor (supplementary material Fig. S4A). Next, the total amounts of NICD produced from N1, N12 and N1^{V1744G} (Huppert et al., 2000) were evaluated in the absence or presence of the proteasome inhibitor Lactacystin (Lac). In the absence of Lac, the amount of NICD accumulated in N12-expressing cells was half of that present in HEK293 expressing N1, independent of plasmid concentration (supplementary material Fig. S4B,C). The addition of the inhibitor Lac significantly increased the overall amount of myc-tagged N1ICD in HEK293 cells expressing wild-type N1, N12 or N1^{V1744G}, a mutation producing a degradable NICD species that, when homozygous, led to a strong phenotype in endothelial cells (Huppert et al., 2000) but not in the somite (Huppert et al., 2005). Nevertheless, the level of N2ICD in N12-expressing HEK293 cells in the presence of Lac only reaches ∼75% of N1ICD levels (supplementary material Fig. S4C), suggesting that both the cleavage of N12 and the stability of N2ICD released from such an allele is reduced compared with the wild-type N1. Unfortunately, owing to the lack of an epitope-specific antibody recognizing cleaved Notch2, we could not perform similar experiments for N1ICD in N21 cells.

Differential accumulation of NICD impacts Notch signaling in two dosage-sensitive tissues: cardiac/endothelial cells (N12) and marginal zone B cells (N21)

Based on these results, we reasoned that dosage-sensitive tissues might not tolerate a single N21 or N12 allele if the respective production of N1ICD and N2ICD from these loci is reduced. To test this, we crossed N1$^{12/12}$ sire with either N1$^{+/-}$ or N1$^{+/V1744G}$ dams (Table 1). Out of 21 pups born to N1$^{+/-}$ mothers, not one had the

Development (2015) 142, 2452-2463 doi:10.1242/dev.125492

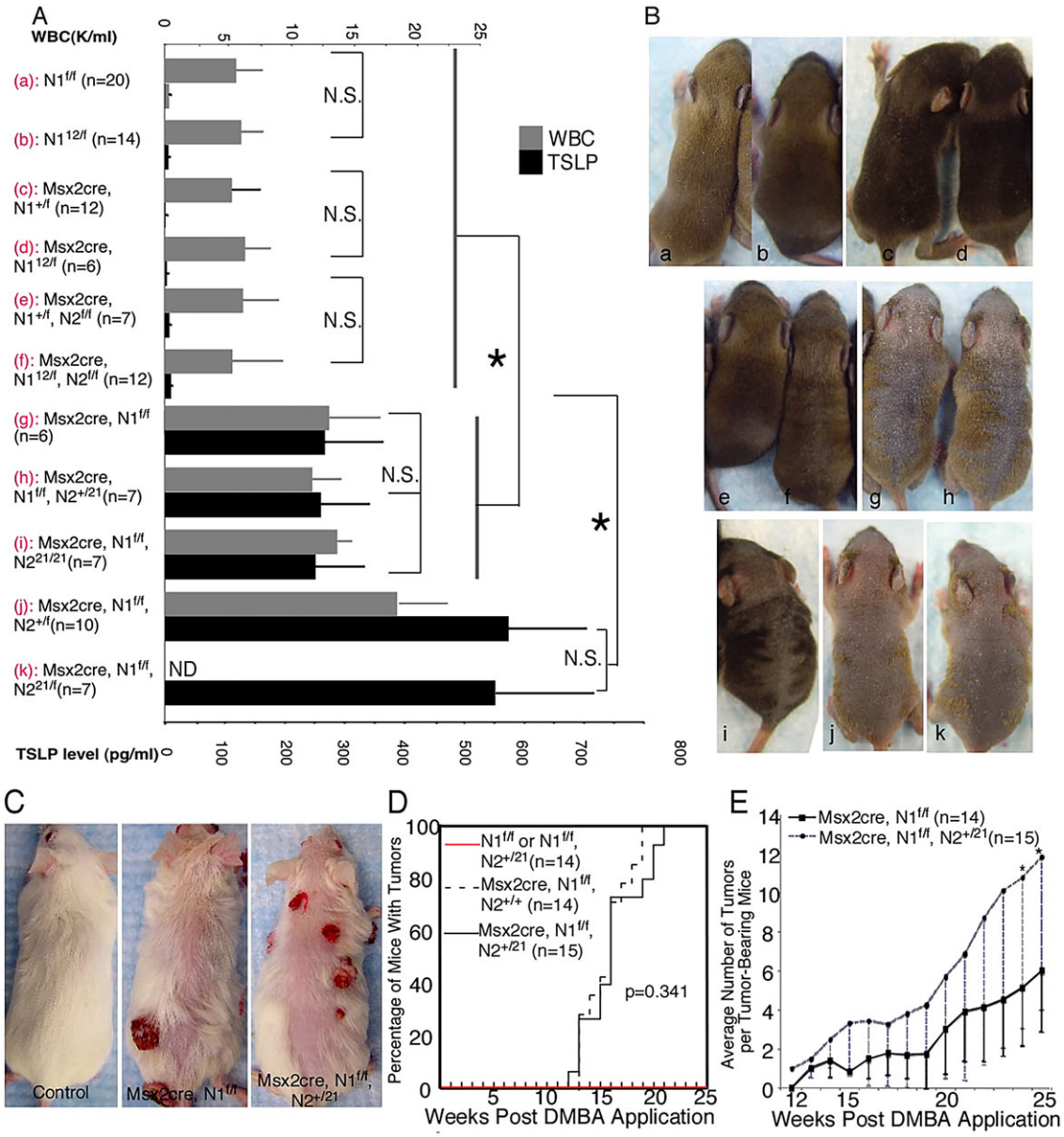

Fig. 4. No significant functional difference could be observed between N1ICD and N2ICD in maintaining skin barrier function and promoting tumorigenesis. (A,B) The loss of the ICD from Notch1 locus, but not from Notch2 locus, disrupts the normal skin barrier function and leads to increased TSLP production and WBC count (A) as well as an obvious skin phenotype (B); the presence of ICD1 or ICD2 in the *Notch1* locus, but not *Notch2* locus, restores the normal skin barrier function (A,B). ND, not determined; N.S., not statistically significant. (C-E) The presence of N1ICD under the control of the N2 locus could not prevent animals that lost wild-type Notch1 from developing carcinomas after DMBA treatment. Error bars represent s.d. *P<0.05.

genotype $N1^{12/-}$. Further analysis revealed that these embryos were recovered at expected frequency before embryonic day (E) 10, but displayed phenotypes in endothelial cells (pale yolk sac and lack of vascular development) from E10 onwards (Fig. 6A, Table 1) (Huppert et al., 2000; Krebs et al., 2000; Liu et al., 2011). Furthermore, if the N^{12} allele provides less NICD than does N1, but more NICD than does $N1^{V1744G}$, one would expect survival of $N1^{12/V1744G}$ embryos to be better than $N1^{V1744G/V1744G}$, which die at E10.5 (Huppert et al., 2000). Indeed, these embryos fared better, with a third (23/79) of $N1^{12/V1744G}$ pups surviving to birth (but only 2/23 surviving at weaning). *In utero*, a high fraction of $N1^{12/V1744G}$ embryos displayed vascular phenotypes, several surviving past E15.5 but failing to thrive shortly thereafter (Table 1; data not shown).

These data could indicate that N12 is a weak allele of *Notch1*, which, though stronger than $N1^{V1744G}$, is insufficient in dosage-sensitive endothelial cells (Theodoris et al., 2015). Alternatively, the composition of the N2ICD may result in failure to activate key target genes (or result in ectopic activation of deleterious genes). To differentiate between these two hypotheses, we isolated ToPro 3^-, $CD31^+$, $CD45^-$ endothelial cells by fluorescence-activated cell sorting (FACS) from E9.5 embryos of the genotypes $N1^{+/+}$, $N1^{+/12}$, $N1^{+/V1744G}$, $N1^{12/V1744G}$, $N1^{+/-}$ and $N1^{12/-}$, purified total RNA and performed RNA sequencing (RNA-Seq) to determine the gene expression profile from each of the genotypes (see Materials and methods). We reasoned that if the latter hypothesis is true, the transcriptome of endothelial cells containing N2ICD would cluster together and that N1ICD and N2ICD 'signatures' would be present

Development (2015) 142, 2452-2463 doi:10.1242/dev.125492

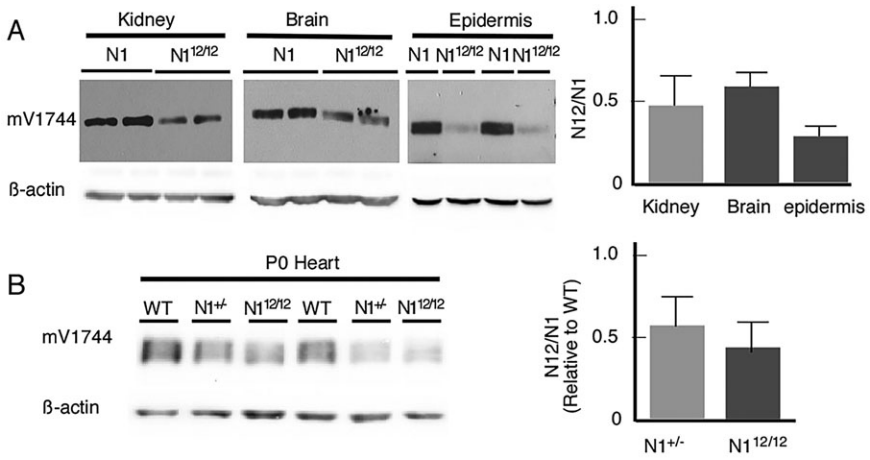

Fig. 5. The levels of cleaved N1ICD in $N1^{12/12}$ animals were reduced to a different degree in different tissues compared with their wild-type counterparts. (A) Comparison of cleaved N1ICD level in the kidney, brain and dermis in newborn wild-type and $N1^{12/12}$ animals. (B) Comparison of cleaved N1ICD level in the heart in newborn wild-type, $N1^{+/-}$ and $N1^{12/12}$ animals. Error bars represent s.d.

in the dataset. Alternatively, all the alleles would be clustered according to 'strength' of signal and would not contain a NICD paralog-specific 'signature'. We used GeneSpring Bioinformatics software to analyze the RNA-Seq data and an unsupervised hierarchical clustering algorithm resulted in the formation of an allelic series ordered based on decreasing strength: the samples containing $N1^{+/+}$, $N1^{+/12}$ and $N1^{+/V1744G}$ clustered near each other, whereas those with the genotypes $N1^{+/-}$, $N1^{12/V1744G}$ and $N1^{12/-}$ showed altered gene expression and increased hypoxic signature (996 genes; Fig. 7A). Given the role of Notch signaling to control endothelial stalk-tip cell-fate decisions, we analyzed the RNA-Seq data to identify if there were any changes in stalk-tip gene expression present in our samples. Using the tip-cell marker VegfR3 (Flt4 – Mouse Genome Informatics) as an anchor, we identified 155 genes trending with a tip-cell signature [including VegfR2 (Kdr – Mouse Genome Informatics), VegfR3, Unc5b, Pdgfrb] in the samples $N1^{+/+}$, $N1^{+/12}$ and $N1^{+/V1744G}$, which also clustered according to 'strength' (Fig. 7B). This hierarchy, and the failure to identify a N2ICD transcriptional signature in this dataset, supported the hypothesis that the endothelial phenotype might be due to reduced N2ICD levels and not composition. Interestingly, when we clustered genes that also display dosage sensitivity in human induced pluripotent stem cell (iPSC)-derived endothelial cells (Theodoris et al., 2015), no clear pattern emerged (Fig. 7C).

To confirm that the N12 allele is hypomorphic, we investigated whether haploinsufficient cardiac phenotypes associated with *Notch1* (de la Pompa, 2009; de la Pompa and Epstein, 2012; Garg et al., 2005; Nus et al., 2011) are evident in the surviving $N1^{+/12}$, $N1^{12/V1744G}$ and $N1^{12/12}$ mice (Table 2; Fig. 6B). Surviving $N1^{12/V1744G}$ and $N1^{12/12}$ mice displayed various cardiac phenotypes that included, with variable penetrance, pulmonary valve stenosis, ventricular septal defects (VSDs) and right ventricular hypertrophy (Table 2). To define the penetrance and severity of the cardiac phenotypes on an inbred background, we crossed B6 males with $N1^{+/12}$ F1 females for ten generations, at which time we bred $N1^{+/12}$ pairs. Strikingly, only one $N1^{12/12}$ pup survived in 114 live births (74 were $N1^{+/12}$ and 39 were $N1^{+/+}$). By contrast, $N1^{12/12}$ embryos constituted ~25% of the litters examined at E9.5, E14.5 and E18.5. All five E18.5 $N1^{12/12}$ embryos from this background that we examined histologically had VSDs (Fig. 6D). These results are consistent with N12 being a hypomorphic allele, most likely as a result of dosage sensitivity, which can be modified by the strain background.

Development and homeostasis of marginal zone B (MZB) cells in the marginal zone (MZ) of the spleen are Notch2-dependent processes (Fig. 8A) (Arnon et al., 2013; Hao and Rajewsky, 2001; Simonetti et al., 2013; Tanigaki et al., 2002) displaying dosage sensitivity: only ~10% of the expected numbers of MZB cells were present in *Notch2* heterozygote spleens (Saito et al., 2003; Witt et al., 2003). To determine where Notch2 is activated and ascertain what choices are made by Notch2 heterozygote cells, we analyzed the distribution of YFP^+ cells isolated from NIP2::Cre^{LO}; ROSA YFP mice (Liu et al., 2013), which are heterozygous for Notch2 but the inactive allele releases Cre recombinase when its ECD is activated by ligand. Cre recombines and activates YFP in cells that experience Notch2 activation and YFP expression is inherited by their descendants. We used flow cytometry to examine YFP expression in T1 ($CD23^-$, $CD21^-$, IgM^+), T2 ($CD23^+$, $CD21^-$,

Table 1. The N12 allele fails to rescue an N1 null and weakly improves survival and vascular phenotypes of the lethal $N1^{V1744G}$ allele

	Number of embryos/pups (phenotype if found dead)					
Stage	Total (litters) for $N1^{12/12}$ $N1^{+/-}$	$N1^{12/+}$	$N1^{12/-}$	Total (litters) for $N1^{12/12}$ $N1^{+/VG}$	$N1^{12/+}$	$N1^{12/VG}$
E9.5	47 (7)	24	23	24 (4)	11	13
E10.5	64 (7)	37	27	6 (1)	1	5 (1 pale yolk sac, cardiac edema, fewer somites)
E11.5	9 (1)	6	3 (necrotic)	12 (1)	8	4 (necrotic, pale yolk sac)
E12.5	8 (2)	5	3 (necrotic)	10 (1)	7	3
E13.5	4 (1)	3	1 (necrotic)	ND	ND	ND
E15.5	ND	ND	ND	11 (1)	5	6 (2 necrotic, 1 absorbed)
E16.5	ND	ND	ND	6 (1)	3	3 (2 necrotic, 1 absorbed)
E18.5	ND	ND	ND	7 (2)	6	1
P0	21 (6)	21	0	79 (10)	56 (2 dead)	23 (3 dead)
P21	21 (6)	21	0	25 (4)	23	2 (1 dead)

ND, not determined.

Development (2015) 142, 2452-2463 doi:10.1242/dev.125492

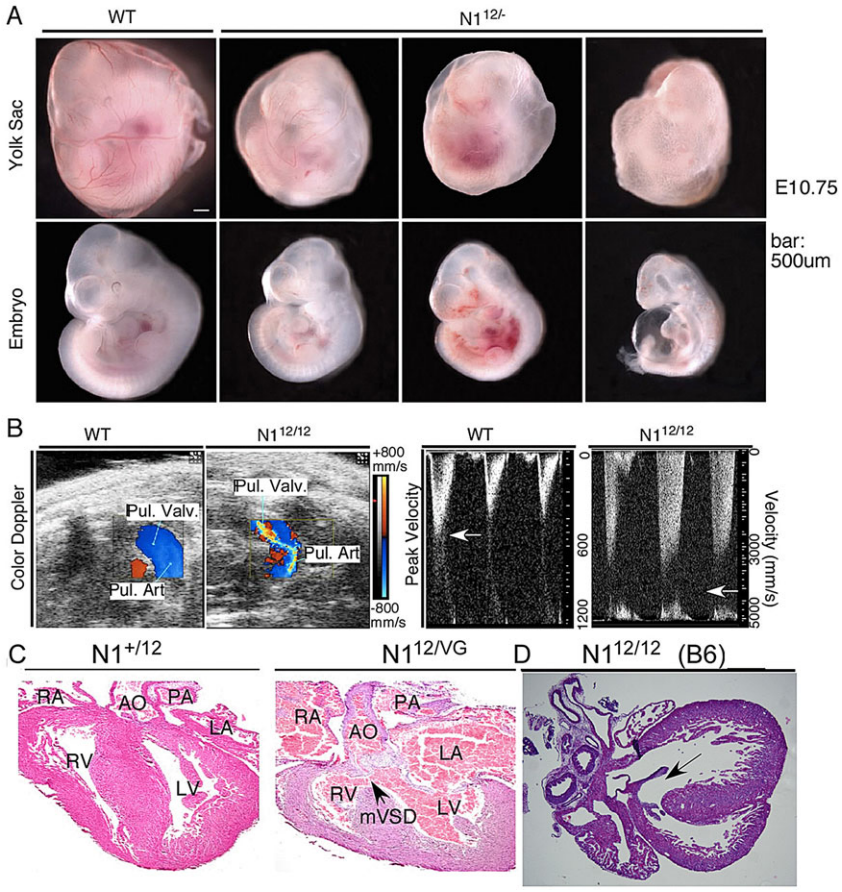

Fig. 6. N12 is weaker than N1 in the cardiovascular system. (A) Unlike wild-type or $N1^{+/-}$ embryos, $N1^{12/-}$ embryos display a range of vascular developmental defects at E10.5, leading to embryonic lethality. (B) Doppler interrogation reveals pulmonary valve stenosis in $N1^{12/12}$ animals. Blood flow across the pulmonic valve in wild-type mice is laminar, as indicated by the uniformly blue color-coded velocity of flow across the pulmonary valve and artery. By contrast, the flow is turbulent and accelerated in an $N1^{12/12}$ mouse, as indicated by the multi-colored flow and increased peak velocity in the pulsed Doppler tracings (arrows). Pul. Art., pulmonary artery; Pul. Valv., pulmonary valve. (C) Histological analyses of hearts from newborn $N1^{12/VG}$ mice reveal membranous ventricular septal defects (mVSD), as indicated by the arrow. AO, aorta; LA, left atrium; LV, left ventricle; PA, pulmonary artery; RA, right atrium; RV, right ventricle. (D) Histological examination of a representative E18.5 heart from congenic C57/Bl6 $N1^{12/12}$ embryos. Arrow indicates the presence of a ventricular septal defect (VSD).

IgM^+), follicular B cell (FoB) ($CD23^+$, $CD21^-$, IgM), marginal zone progenitor (MZP; $CD23^+$, $CD21^+$, IgM^+) and MZB ($CD23^-$, $CD21^+$, IgM^+) populations (Fig. 8B,B′). As expected, we found YFP expression in MZP and MZB cells, but, surprisingly, FoB cells were labeled instead of T2 cells (Fig. 8E,F).

To determine whether NICD composition made a contribution, we analyzed MZB cell numbers in the spleens of wild-type, $N2^{21/21}$, $N2^{+/21}$, $N2^{+/-}$ and $N2^{21/-}$ mice (Fig. 8B,B′). Although variable, $N2^{21/21}$ spleens contained as few MZB cells as N2 heterozygotes (~20% of wild type; Fig. 8C,D) and $N2^{21/-}$ contained even fewer. A similar reduction in MZP cells was also detected (Fig. 8C). To ascertain whether the defects we detected reflected the composition of N1ICD, we quantified the number of MZB cells generated from *CD19-Cre; Rosa-NICD* animals, in which N1ICD was overexpressed (Murtaugh et al., 2003). If N1ICD were not competent to interact with Maml1 and drive the T2-to-MZP transition, we would not expect to see an increase in the number of MZB or MZP cells. Instead, we observed an approximately threefold increase in MZP cells and a ~2.5-fold increase in MZB cells (supplementary material Fig. S5), similar to the effect of N2ICD (Hampel et al., 2011). These findings further strengthen the notion that the NICDs are interchangeable and the N1ICD is efficient in driving the MZP cell fate.

DISCUSSION

An understanding of how qualitative and quantitative aspects of Notch signaling govern gene expression output remains elusive (see Boareto et al., 2015; Shaya and Sprinzak, 2011; Sprinzak et al., 2010). Notch1 and Notch2 have been shown to have different contributions in certain cellular, developmental and disease contexts, while having equal contributions in others. In this and a previous study (Liu et al., 2013), we failed to find support for the notion that NICD composition differentiates Notch1 from Notch2. Our data instead point to the conclusion that strength (defined here as the ultimate number of intracellular domain of NICD molecules reaching the nucleus, integrating ligand-mediated release and nuclear translocation) and duration (half-life of NICD-RBPjk-MAML-DNA complexes, integrating cooperativity and stability dependent on shared sequence elements) are most likely the factors that underlie many of the differences between Notch1 and Notch2 in many contexts. This conclusion does not rule out the possibility that the composition of N3ICD (and N4ICD) can deliver functions (e.g. Zheng et al., 2013). The differences in Notch1/2 signaling cannot be explained by virtue of differences in their amino acid composition.

We show that on a mixed genetic background, mice were insensitive to the composition of the NICD. Even organs or cell types that evolved using predominantly one receptor, such as T cells, hematopoietic stem cells, lung or the inner ear can effectively utilize the orthologous ICD, arguing against the possibility that sequence diversity between Notch1 and Notch2 arose to accommodate tissue-specific partners. In addition to this general conclusion, several interesting details have emerged. First, these alleles are deficient relative to the parental Notch allele because the choice of scissile bond by γ-secretase appears to be impacted by the composition of intracellular juxtamembrane amino acids, affecting the overall steady state level of N1ICD. The degree of this impact varies based on the cell type, perhaps owing to the tissue-specific composition of γ-secretase (Jorissen and De Strooper, 2010). This led us to examine the effect of swapping alleles across a null allele in tissues known for dosage sensitivity. The $N1^{12}$ allele was unable to support endothelial

Development (2015) 142, 2452-2463 doi:10.1242/dev.125492

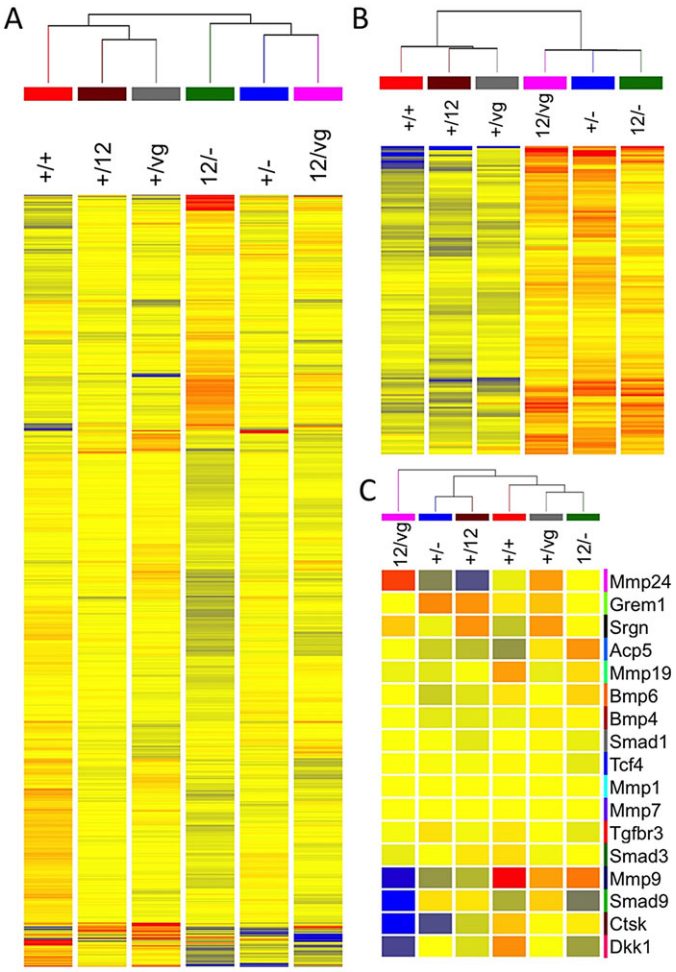

Fig. 7. Transcriptome analysis of endothelial cells generated from a Notch allelic series. (A) Hierarchical clustering analysis depicting the segregation of transcripts isolated from endothelial cells sorted from E9.5 embryos harboring different Notch alleles. Note clear separation of two categories: a group consisting of at least one wild-type *Notch1* allele and a weak Notch allele, and a group containing a single *Notch1* allele or combinations of weak Notch alleles in endothelial cells. (B) Pearson correlation analysis with a cut-off range [0.8,1.0] was used to identify genes that trend with the tip marker gene Vegfr3. A hierarchical clustering analysis was performed which showed that the alleles $Notch1^{+/-}$, $N1^{12/vg}$ and $N1^{12/-}$ share a similar expression signature distinct from the cells expressing $Notch1^{+/+}$, $Notch1^{+/12}$ and $Notch1^{+/vg}$ alleles. Tip cell characteristics segregate with a reduced Notch signaling environment. (C) Hierarchical clustering analysis of mouse endothelial genes that were differentially regulated in iPSC-derived Notch1 heterozygous endothelial cells exposed to shear stress (Theodoris et al., 2015). These genes did not segregate based on Notch signaling strength in mouse embryonic endothelial cells.

development across a null, but in trans-heterozygote combination with another weak *Notch1* allele ($N1^{V1774G}$) viability was somewhat improved. The existence of *Notch1* alleles differing in strength allowed us to ask whether introduction of the N2ICD resulted in a specific gene signature. Our transcriptome analyses failed to detect such a signature, instead characterizing the $N1^{12}$ allele as a weak *Notch1* allele. It is worth noting that our analysis in mouse endothelial cells did not support the conclusion that Notch heterozygote iPSC-derived endothelial cells activate an ossification program (Theodoris et al., 2015), similar to the response of smooth muscle cells that have lost Notch signals (Briot et al., 2014). Instead, we observe an elevated tip-cell signature in Notch heterozygotes, consistent with the majority of published studies exploring the role of Notch in endothelium (Benedito et al., 2009; Hellstrom et al., 2007; Jakobsson et al., 2010).

Notch2 activation within the follicular compartment by Dll1-expressing fibroblastic reticular cells (Fasnacht et al., 2014) triggers a Notch2 signal strength-dependent conversion of precursor cells to MZB cells and the subsequent migration to the marginal zone. The N^{21} allele behaved as a weak *Notch2* allele during MZB cell differentiation. This observation can fit any one of three models. First, apoptosis eliminates MZPs with low Notch2 activity, resulting in fewer MZB cells. Second, a developmental fate switch relying on Notch2 shunts MZP cells with low Notch2 activity to follicular B cells (FoB) instead of MZB cells. Third, Notch2 is required for the retention of MZB cells in the marginal zone and for the maintenance of MZB cell identity. In the third model, after the effects of Notch2 activation declines the cells return to the follicle and become indistinguishable from FoB cells, or are re-stimulated and move back to the MZ (Simonetti et al., 2013). Evidence for this comes from the rapid turnover kinetics within the MZ (Arnon et al., 2013; Simonetti et al., 2013) and the persistence of MZB cells in conditional $Rag2^{-/-}$ mice, suggesting replenishment of MZB cells from a FoB cell pool (Hao and Rajewsky, 2001; Srivastava et al., 2005) in a Notch2-dependent process. The rapid expulsion of MZB cells into the circulation when Notch2-blocking antibodies are added (Simonetti et al., 2013) is consistent with this possibility as well. Our linage tracing of NIP2::Cre^{LO} B cells show labeling in the FoB cell compartment, consistent with either model 2 (shunting of cells with lower Notch2 activity to FoB) or model 3 (Notch2-dependent cycling between FoB and MZB cells), but not with apoptosis removing cells with lower Notch2 activity. Lack of YFP expression in T2 cells indicates that they do not experience substantial NIP2::Cre^{LO} activation (Liu et al., 2015).

Importantly, the strain background modified dosage effects in endothelial and cardiac tissue. $N1^{12/12}$ mice are viable and display no overt phenotype on a mixed background (Fig. 1). However, moving the N^{12} allele into the congenic B6 background increased the penetrance and severity of VSDs in $N1^{12/12}$ animals to such a degree that only one of 114 live births survived to adulthood. This genetic enhancement of weak *Notch1* alleles might play an important role in disease etiology in human as well. Identifying Notch1 cardiac modifiers could prove relevant both as a predictor of cardiac health and as a path to the identification of therapeutically exploitable pathways protecting these mice from VSDs in the mixed background. In addition, our data warrant reinterpretation of clinical findings reporting differential outcomes segregating with Notch1 or Notch2 (Boulay et al., 2007; Chu et al., 2011; Fan et al., 2004; Graziani et al., 2008; Parr et al., 2004). Our data suggest that such differences likely reflect the overall strength of Notch signals, and indicate that a careful evaluation of which allele is 'stronger' may indicate the preferred direction of an intervention (to increase or decrease pathway strength) instead of a focus on allele composition.

MATERIALS AND METHODS

Mice

The generation and genotyping of the N12 and N21 mice is described by Liu et al. (2013). N1V1744G (Huppert et al., 2000), *Notch1* null ($N1^{-}$; Conlon et al., 1995), *Notch2* null ($N2^{-}$; BayGenomics gene trap lines LST103), $N1^{f/f}$ (Notch1tm2Rko; Yang et al., 2004), $N2^{f/f}$ (Kiernan et al., 2005), Msx2-Cre (Pan et al., 2004) and $Rosa^{Notch}$ (Murtaugh et al., 2003) mice were genotyped as described. All mice were harvested either in the animal facility of Washington University or in the animal facility at Cincinnati Children's Hospital Medical Center (CCHMC). Washington

Development (2015) 142, 2452-2463 doi:10.1242/dev.125492

Table 2. Cardiac phenotypes associated with N12 and Notch21 alleles

	Adult mice echocardiography data		Heart histology at P1	
Genotype	Number of mice analyzed	Number of mice with cardiac phenotype	Number of mice analyzed	Number of mice with cardiac phenotype
N1+/+ (B6/CD1)	1	0	ND	ND
N1+/12 (B6/CD1)	3	0	15	0
N112/12 (B6/CD1)	4	3	5	3 (VSD)
N112/12 (B6*)	1	?	5 (embryos)	5 (VSD)
N112/VG (B6/CD1)	2	1	7	7 (VSD)
N221/21 (B6/CD1)	4	0	ND	ND

*In the B6 background, $N1^{+/12}$ parents produced E18.5 embryos with $N1^{12/12}$ genotype at the expected Mendelian distribution but only one pup out of 114 live births was $N1^{2/12}$. Thus far, 100% of E14.5 and E18.5 $N1^{12/12}$ embryos in the B6 background have VSDs.
ND, not determined.

University and CCHMC Animal Studies Committees approved all experimental procedures.

Immunohistochemistry

All immunohistochemistry procedures, including Hematoxylin and Eosin (H&E) staining, were performed as described by Liu et al. (2011). Briefly, tissues were dissected from euthanized animals, fixed with 4% paraformaldehyde in 1× PBS at 4°C overnight (newborn hearts were fixed for around one week) with constant agitation and then washed thoroughly with 1× PBS. For paraffin sections, the tissues were further dehydrated with 30%, 50% and 70% ethanol and embedded in paraffin. Before antibody staining, the paraffin sections were deparaffinized with a xylene substitute and rehydrated with 95%, 70%, 50% and 30% ethanol. Heat-mediated antigen retrieval was achieved by autoclaving sections at 121°C for 20 min in 10 mM sodium citrate (pH 6.0). For frozen sections, tissues were soaked in 30% sucrose in 1× PBS overnight and embedded in Tissue-Tek OCT

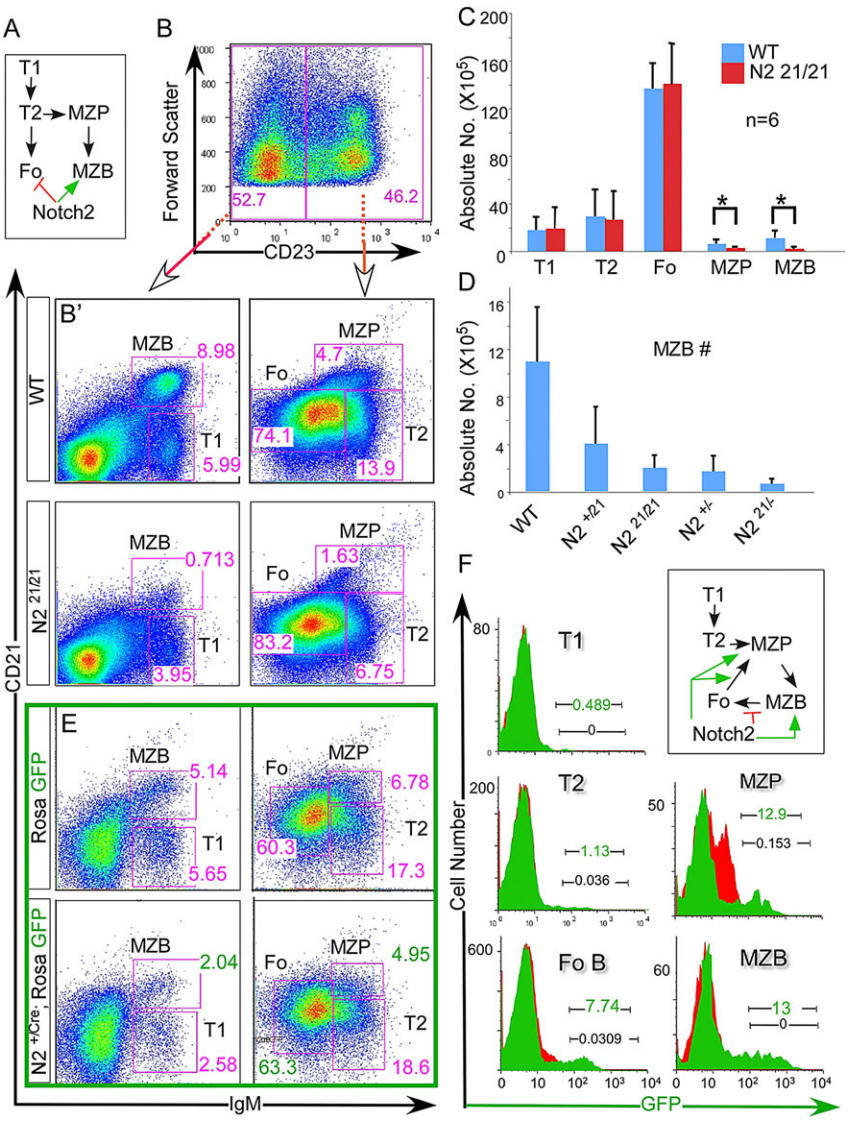

Fig. 8. $N2^{21}$ is weaker than N2 in promoting marginal zone B cell development in the spleen. (A) A model depicting the development of MZB and follicular B cells (Fo) in the spleen. Notch2 promotes the development of MZP and MZB cells but inhibits the development of Fo cells. (B,B′) Strategies to quantify the different populations of spleen B cells with flow cytometry. (C) The spleen of $N2^{21/21}$ mice has reduced number of MZP and MZB cells. (D) The number of MZB cells correlates with the dosage of Notch2 activity in the spleen of wild type, $N2^{+/21}$, $N2^{21/21}$, $N2^{+/-}$ and $N2^{21/-}$, suggesting the absence of qualitative difference between N2ICD and N1ICD. (E,F) Fate mapping of cells with reduced Notch2 activity using N2IP::Cre, Rosa GFP mice reveals strong GFP labeling in MZP, MZB and Fo cells, suggesting a possible identity conversion among the three populations of cells depending on the strength of Notch2 activity (model in F). Error bars represent s.d. *P<0.05.

Development (2015) 142, 2452-2463 doi:10.1242/dev.125492

compound. Antigen retrieval was achieved by permeabilizing sections at room temperature in 1× PBS with 0.1% Triton X-100 for 20 min. The following primary antibodies were used: rabbit anti-keratin 19 (ab52625, Abcam; 1:100) on liver paraffin sections; rabbit anti-Notch1 (3608, Cell Signaling; 1:200), rabbit anti-Notch2 (5732, Cell Signaling; 1:400), rabbit anti-Notch3 ICD (gift from Dr Urban Lendahl, Karolinska Institute, Stockholm, Sweden; 1:200), chick anti-K14, -K1 and -filaggrin (generous gifts from Dr Julie Segre, National Human Genome Research Institute, NIH, Bethesda, MD, USA; 1:400, 1:400 and 1:200, respectively) and rat anti-β4 integrin (553745, BD Biosciences; 1:100) on frozen skin sections. The primary antibodies were detected with the following secondary antibodies: HRP-conjugated anti-rabbit followed by DAB color reaction (for Keratin 19); Cy3-conjugated donkey anti-rabbit; Alexa Fluor 488-conjugated donkey anti-chick; Cy5-conjugated donkey anti-rat (all from Jackson ImmunoResearch). Inner ears were dissected under a stereomicroscope, fixed and stained with FITC-conjuated phalloidin (R&D Systems). All immunofluorescence images were captured with an ApoTome microscope (Zeiss) and bright-field images taken with a Z3 microscope (Zeiss). Images were further processed with Adobe Photoshop CS2 and Canvas X.

Diagnosis of congenital heart defects

Neonatal pups were collected within hours of birth to prevent cannibalization of animals that have serious congenital heart defects. The pups were euthanized by decapitation. The thorax was fixed in 10% neutral-buffered formalin. The hearts were then dissected, embedded in paraffin, and entirely sectioned in the frontal plane at 6 µm thickness. A pediatric cardiologist inspected all the sections to assess the phenotype of the hearts, as previously described (Winston et al., 2010).

Cell culture, transfection and western blot

Cell culture, transfection and western blot from tissue lysate or cultured cells were performed as described by Liu et al. (2013). The following primary antibodies were used: rabbit monoclonal anti-V1744 antibody (4147, Cell Signaling; 1:1000); mouse anti-6Xmyc tag antibody (9E10 ascites, homemade; 1:2000); mouse anti-β-actin antibody (AC-15, Sigma; 1:10,000).

Flow cytometry analysis

Flow cytometry was performed as previously described (Liu et al., 2013). Briefly, the spleen and the thymus were mechanistically disrupted and filtered using a nylon mesh. Bone marrow cells were flushed from the femur and tibia bones. Red blood cells in the samples were lysed with 1× lysis buffer (0.826% NH_4Cl, 0.1% $KHCO_3$, 0.002% EDTA) by pipetting up and down for 45 s. The samples were pelleted at 2000 rpm (400 ***g***) for 5 min, resuspended in 1× FACS staining buffer (3% BSA in 1× PBS), incubated with proper antibodies on ice for 30 min, washed and filtered through 40 µm membrane for flow cytometry analysis. The following antibodies were used at 1:100: CD44, CD25, CD21, CD23, IgM, Sca-1, c-Kit (all Biolegend), CD4, CD8, B220 and Thy1.2 (all BD Biosciences). Data were collected on BD FACScan with FlowJo Collectors' Edition and analyzed using FlowJo software (TreeStar).

FACS of embryonic endothelial cells

For FACS analyses, 9.5-day-old embryos were dissected, washed in 1× PBS and digested in 1 ml pre-warmed Williams E medium containing 1 mg Collagenase (Sigma) at 37°C with vigorous shaking for 30 min; at the same time, genotyping PCR was performed with yolk sac. Digested embryo samples were further lysed with 1× Red Blood Cell lysis buffer (0.826% NH_4Cl, 0.1% $KHCO_3$; note that EDTA is omitted to avoid activating Notch), pelleted, resuspended in 1× FACS staining buffer (3% BSA in 1× PBS), then stained with FITC-conjugated CD31 (102506, Biolegend; 1:100; PECAM) and PerCP-Cy5.5-conjugated CD45 (103131, Biolegend) on ice for 30 min, washed and resuspended in 1× FACS staining buffer containing 2 µM To-Pro-3 iodide (T3605, Life Technologies) and left on ice until genotyping results were obtained. Samples from embryos with the same genotype were then pooled for FACS to increase the cell number and reduce FACS time. To-Pro 3^- (live), $CD45^-$ (non-lymphocytes) and $CD31^+$ endothelial cells were sorted directly into lysis buffer from Qiagen RNeasy Micro Kit that was supplemented with 2-mercapitoethanol using a highly modified Beckman Coulter MoFlo and were then kept at −80°C until ready for RNA purification.

HSC culture

LSKSLAM cells were sorted from adult murine bone marrow depleted of cells expressing the following lineage markers: CD1, CD3, CD8a, CD5, CD11b, B220, GR1 and TER-119. LSKSLAM cells were then obtained using FACS on an ARIA Cell Sorter (BD Biosciences), based on positive Sca-1 (Ly6a – Mouse Genome Informatics), Kit and CD150 (Slamf1 – Mouse Genome Informatics) expression but negative CD48 expression. LSKSLAM cells (250-500) were cultured in non-tissue culture wells (Falcon, BD Biosciences) previously incubated with PBS plus fibronectin fragment CH-296 (Takara Shuzo Co.) at 5 µg/ml solutions, and containing either Notch ligand $Delta1^{ext\text{-}IgG}$ at 5 µg/ml, $Jagged1^{ext\text{-}IgG}$ at 20 µg/ml, or human IgG_1 (Sigma). Construct, protein generation and quantitative evaluation in cell culture of these ligands have all been described previously (Dallas et al., 2005). LSKSLAM cells were cultured for 14 days as previously described (Varnum-Finney et al., 2011), stained with monoclonal antibodies, and analyzed on a Canto-2 cytometer (BD Biosciences).

Total RNA purification and RNA-Seq analysis

Total RNA from sorted cells was purified using the Qiagen RNeasy Micro Kit following manufacturer's protocols. RNA quality and concentration was determined using an Agilent 2100 Bioanalyzer. The RNA-Seq libraries were generated by the CCHMC Gene Expression Core using a Nugen Ovation RNA-Seq System V2 and Nextera DNA Sample Prep Kit according to manufacturer's protocols. Sequencing was carried out using the Illumina HiSeq 2000 system according to Illumina protocols. To analyze the RNA-Seq data, we used an approach that is similar to the model developed by Mortazavi et al. (2008) in their ERANGE (http://woldlab.caltech.edu/rnaseq/) RNA-Seq analysis pipeline. Per-spot sequence reads were aligned allowing up to two mismatches and ten multiple mappings to both genome and transcriptome targets. We used Bowtie (http://bowtie-bio.sourceforge.net/index.shtml) and Tophat (https://ccb.jhu.edu/software/tophat/index.shtml) for genome and transcriptome alignments. Analysis of the data was conducted using Genespring 12.6 and the RNA-Seq data was RPKM normalized and filtered on expression, removing those that failed to have a minimum of five RPKM in at least two samples. An ANOVA statistical test was applied to find differentially expressed genes ($P \leq 0.05$). The data have been deposited in the Gene Expression Omnibus database (GSE69276).

Quantitative RT-PCR analysis

Quantitative RT-PCR analyses to compare the expression levels of various marker genes in E18.5 embryonic lung were performed as described by Morimoto et al. (2012).

Chemical skin carcinogenesis study

This was performed as described by Demehri et al. (2009) and Nicolas et al. (2003). Briefly, 15 animals for each genotype were treated once on the dorsal skin after shaving with 200 µl acetone containing 25 µg DMBA (Sigma) at the age of 6-10 weeks. The appearance and number of tumors was monitored and recorded weekly thereafter.

TSLP measurement and WBC count

Serum TSLP level was determined with Quantikine mouse TSLP ELISA Kit (R&D Systems). WBC counts were determined with Hemavet 950 Analyzer (Drew Scientific) after fresh blood was diluted in an equal volume of 10 mM EDTA in 1× PBS.

Echocardiography

Echocardiography was performed on conscious, adult mice using a Vevo 2100 Imaging System (VisualSonics, Toronto, Canada) equipped with the MS-400 30 MHz linear-array transducer. Parasternal views in the long and

Development (2015) 142, 2452-2463 doi:10.1242/dev.125492

short axes of the heart were obtained with a handheld technique to collect 2D images. Additional color and pulsed-wave Doppler images of the right ventricular outflow tract, pulmonary valve and artery were obtained to diagnose and quantify the degree of pulmonic valve stenosis.

Statistics

Student's *t*-test was employed to determine the *P*-value unless otherwise specified.

Acknowledgements

We thank Washington University Siteman Cancer Center Flow Cytometry Core for allowing us to use their flow cytometer and for their assistance with FACS; Genome Technology Access Center (GTAC) for assistance with Agilent Bioanalyzer analysis; and Mouse Cardiovascular Phenotyping Core for performing echocardiography. We also thank the CCHMC Gene Expression Core for assistance in generating the RNA-Seq libraries. We also want to thank Dr Sung-Ho Huh for technical help in analyzing inner ear samples.

Competing interests

The authors declare no competing or financial interests.

Author contributions

Z.L. and R.K. conceived the project and wrote the manuscript; Z.L. performed most of the experiments; E.B. performed RNA-Seq analysis and edited the manuscript; B.V.-F. and I.B. performed HSC *in vitro* culture study; C.Z. and A.Z. helped with inner ear and skin immunostaining analyses; P.Y.J. analyzed congenital heart defects; M.M. carried out the lung cell marker study.

Funding

This work was supported by the National Institutes of Health [RO1G55479 to Z.L., C.Z., A.Z., M.M. and R.K.; U01 HL100395 to B.V.-F. and I.B.; HL105857 to P.Y.J.]; the William K. Schubert Chair for Pediatric Research [R.K. and E.B.]; an Established Investigator award from the American Heart Association [P.Y.J.]; and the Lawrence J. & Florence A. DeGeorge Charitable Trust [P.Y.J.]. Deposited in PMC for release after 12 months.

Supplementary material

Supplementary material available online at
http://dev.biologists.org/lookup/suppl/doi:10.1242/dev.125492/-/DC1

References

Arnon, T. I., Horton, R. M., Grigorova, I. L. and Cyster, J. G. (2013). Visualization of splenic marginal zone B-cell shuttling and follicular B-cell egress. *Nature* **493**, 684-688.

Benedito, R., Roca, C., Sörensen, I., Adams, S., Gossler, A., Fruttiger, M. and Adams, R. H. (2009). The notch ligands Dll4 and Jagged1 have opposing effects on angiogenesis. *Cell* **137**, 1124-1135.

Blat, Y., Meredith, J. E., Wang, Q., Bradley, J. D., Thompson, L. A., Olson, R. E., Stern, A. M. and Seiffert, D. (2002). Mutations at the P1′ position of Notch1 decrease intracellular domain stability rather than cleavage by gamma-secretase. *Biochem. Biophys. Res. Commun.* **299**, 569-573.

Boareto, M., Jolly, M. K., Lu, M., Onuchic, J. N., Clementi, C. and Ben-Jacob, E. (2015). Jagged-Delta asymmetry in Notch signaling can give rise to a Sender/Receiver hybrid phenotype. *Proc. Natl. Acad. Sci. USA* **112**, E402-E409.

Boulay, J.-L., Miserez, A. R., Zweifel, C., Sivasankaran, B., Kana, V., Ghaffari, A., Luyken, C., Sabel, M., Zerrouqi, A., Wasner, M. et al. (2007). Loss of NOTCH2 positively predicts survival in subgroups of human glial brain tumors. *PLoS ONE* **2**, e576.

Briot, A., Jaroszewicz, A., Warren, C. M., Lu, J., Touma, M., Rudat, C., Hofmann, J. J., Airik, R., Weinmaster, G., Lyons, K. et al. (2014). Repression of Sox9 by Jag1 is continuously required to suppress the default chondrogenic fate of vascular smooth muscle cells. *Dev. Cell* **31**, 707-721.

Cheng, H.-T., Kim, M., Valerius, M. T., Surendran, K., Schuster-Gossler, K., Gossler, A., McMahon, A. P. and Kopan, R. (2007). Notch2, but not Notch1, is required for proximal fate acquisition in the mammalian nephron. *Development* **134**, 801-811.

Chiang, M. Y., Xu, M. L., Histen, G., Shestova, O., Roy, M., Nam, Y., Blacklow, S. C., Sacks, D. B., Pear, W. S. and Aster, J. C. (2006). Identification of a conserved negative regulatory sequence that influences the leukemogenic activity of NOTCH1. *Mol. Cell. Biol.* **26**, 6261-6271.

Chu, D., Zhang, Z., Zhou, Y., Wang, W., Li, Y., Zhang, H., Dong, G., Zhao, Q. and Ji, G. (2011). Notch1 and Notch2 have opposite prognostic effects on patients with colorectal cancer. *Ann. Oncol.* **22**, 2440-2447.

Conlon, R. A., Reaume, A. G. and Rossant, J. (1995). Notch1 is required for the coordinate segmentation of somites. *Development* **121**, 1533-1545.

Dallas, M. H., Varnum-Finney, B., Delaney, C., Kato, K. and Bernstein, I. D. (2005). Density of the Notch ligand Delta1 determines generation of B and T cell precursors from hematopoietic stem cells. *J. Exp. Med.* **201**, 1361-1366.

de la Pompa, J. L. (2009). Notch signaling in cardiac development and disease. *Pediatr. Cardiol.* **30**, 643-650.

de la Pompa, J. L. and Epstein, J. A. (2012). Coordinating tissue interactions: Notch signaling in cardiac development and disease. *Dev. Cell* **22**, 244-254.

Demehri, S., Liu, Z., Lee, J., Lin, M.-H., Crosby, S. D., Roberts, C. J., Grigsby, P. W., Miner, J. H., Farr, A. G. and Kopan, R. (2008). Notch-deficient skin induces a lethal systemic B-lymphoproliferative disorder by secreting TSLP, a sentinel for epidermal integrity. *PLoS Biol.* **6**, e123.

Demehri, S., Turkoz, A. and Kopan, R. (2009). Epidermal Notch1 loss promotes skin tumorigenesis by impacting the stromal microenvironment. *Cancer Cell* **16**, 55-66.

Fan, X., Mikolaenko, I., Elhassan, I., Ni, X., Wang, Y., Ball, D., Brat, D. J., Perry, A. and Eberhart, C. G. (2004). Notch1 and notch2 have opposite effects on embryonal brain tumor growth. *Cancer Res.* **64**, 7787-7793.

Fasnacht, N., Huang, H.-Y., Koch, U., Favre, S., Auderset, F., Chai, Q., Onder, L., Kallert, S., Pinschewer, D. D., MacDonald, H. R. et al. (2014). Specific fibroblastic niches in secondary lymphoid organs orchestrate distinct Notch-regulated immune responses. *J. Exp. Med.* **211**, 2265-2279.

Fiorini, E., Merck, E., Wilson, A., Ferrero, I., Jiang, W., Koch, U., Auderset, F., Laurenti, E., Tacchini-Cottier, F., Pierres, M. et al. (2009). Dynamic regulation of notch 1 and notch 2 surface expression during T cell development and activation revealed by novel monoclonal antibodies. *J. Immunol.* **183**, 7212-7222.

Fryer, C. J., White, J. B. and Jones, K. A. (2004). Mastermind recruits CycC:CDK8 to phosphorylate the Notch ICD and coordinate activation with turnover. *Mol. Cell* **16**, 509-520.

Garg, V., Muth, A. N., Ransom, J. F., Schluterman, M. K., Barnes, R., King, I. N., Grossfeld, P. D. and Srivastava, D. (2005). Mutations in NOTCH1 cause aortic valve disease. *Nature* **437**, 270-274.

Geisler, F., Nagl, F., Mazur, P. K., Lee, M., Zimber-Strobl, U., Strobl, L. J., Radtke, F., Schmid, R. M. and Siveke, J. T. (2008). Liver-specific inactivation of Notch2, but not Notch1, compromises intrahepatic bile duct development in mice. *Hepatology* **48**, 607-616.

Graziani, I., Eliasz, S., De Marco, M. A., Chen, Y., Pass, H. I., De May, R. M., Strack, P. R., Miele, L. and Bocchetta, M. (2008). Opposite effects of Notch-1 and Notch-2 on mesothelioma cell survival under hypoxia are exerted through the Akt pathway. *Cancer Res.* **68**, 9678-9685.

Groot, A. J., Cobzaru, C., Weber, S., Saftig, P., Blobel, C. P., Kopan, R., Vooijs, M. and Franzke, C.-W. (2013). Epidermal ADAM17 is dispensable for Notch activation. *J. Invest. Dermatol.* **133**, 2286-2288.

Hampel, F., Ehrenberg, S., Hojer, C., Draeseke, A., Marschall-Schroter, G., Kuhn, R., Mack, B., Gires, O., Vahl, C. J., Schmidt-Supprian, M. et al. (2011). CD19-independent instruction of murine marginal zone B-cell development by constitutive Notch2 signaling. *Blood* **118**, 6321-6331.

Hao, Z. and Rajewsky, K. (2001). Homeostasis of peripheral B cells in the absence of B cell influx from the bone marrow. *J. Exp. Med.* **194**, 1151-1164.

Hellstrom, M., Phng, L.-K., Hofmann, J. J., Wallgard, E., Coultas, L., Lindblom, P., Alva, J., Nilsson, A.-K., Karlsson, L., Gaiano, N. et al. (2007). Dll4 signalling through Notch1 regulates formation of tip cells during angiogenesis. *Nature* **445**, 776-780.

Huppert, S. S., Le, A., Schroeter, E. H., Mumm, J. S., Saxena, M. T., Milner, L. A. and Kopan, R. (2000). Embryonic lethality in mice homozygous for a processing-deficient allele of Notch1. *Nature* **405**, 966-970.

Huppert, S. S., Ilagan, M. X. G., De Strooper, B. and Kopan, R. (2005). Analysis of Notch function in presomitic mesoderm suggests a γ-secretase-independent role for presenilins in somite differentiation. *Dev. Cell* **8**, 677-688.

Jakobsson, L., Franco, C. A., Bentley, K., Collins, R. T., Ponsioen, B., Aspalter, I. M., Rosewell, I., Busse, M., Thurston, G., Medvinsky, A. et al. (2010). Endothelial cells dynamically compete for the tip cell position during angiogenic sprouting. *Nat. Cell Biol.* **12**, 943-953.

Jorissen, E. and De Strooper, B. (2010). Gamma-secretase and the intramembrane proteolysis of Notch. *Curr. Top. Dev. Biol.* **92**, 201-230.

Kiernan, A. E., Cordes, R., Kopan, R., Gossler, A. and Gridley, T. (2005). The Notch ligands DLL1 and JAG2 act synergistically to regulate hair cell development in the mammalian inner ear. *Development* **132**, 4353-4362.

Kopan, R. and Ilagan, M. X. G. (2009). The canonical Notch signaling pathway: unfolding the activation mechanism. *Cell* **137**, 216-233.

Kovall, R. A. and Blacklow, S. C. (2010). Mechanistic insights into Notch receptor signaling from structural and biochemical studies. *Curr. Top. Dev. Biol.* **92**, 31-71.

Krebs, L. T., Xue, Y., Norton, C. R., Shutter, J. R., Maguire, M., Sundberg, J. P., Gallahan, D., Closson, V., Kitajewski, J., Callahan, R. et al. (2000). Notch signaling is essential for vascular morphogenesis in mice. *Genes Dev.* **14**, 1343-1352.

Liu, Z., Turkoz, A., Jackson, E. N., Corbo, J. C., Engelbach, J. A., Garbow, J. R., Piwnica-Worms, D. R. and Kopan, R. (2011). Notch1 loss of heterozygosity

causes vascular tumors and lethal hemorrhage in mice. *J. Clin. Invest.* **121**, 800-808.

Liu, Z., Chen, S., Boyle, S., Zhu, Y., Zhang, A., Piwnica-Worms, D. R., Ilagan, M. X. and Kopan, R. (2013). The extracellular domain of Notch2 increases its cell-surface abundance and ligand responsiveness during kidney. *Dev. Cell* **25**, 585-598.

Liu, Z., Brunskill, E., Boyle, S., Chen, S., Turkoz, M., Guo, Y., Grant, R. and Kopan, R. (2015). Second-generation Notch1 activity-trap mouse line (N1IP::CreHI) provides a more comprehensive map of cells experiencing Notch1 activity. *Development* **142**, 1193-1202.

MacGrogan, D., Nus, M. and de la Pompa, J. L. (2010). Notch signaling in cardiac development and disease. *Curr. Top. Dev. Biol.* **92**, 333-365.

McCright, B., Gao, X., Shen, L., Lozier, J., Lan, Y., Maguire, M., Herzlinger, D., Weinmaster, G., Jiang, R. and Gridley, T. (2001). Defects in development of the kidney, heart and eye vasculature in mice homozygous for a hypomorphic Notch2 mutation. *Development* **128**, 491-502.

McCright, B., Lozier, J. and Gridley, T. (2002). A mouse model of Alagille syndrome: Notch2 as a genetic modifier of Jag1 haploinsufficiency. *Development* **129**, 1075-1082.

Morimoto, M., Nishinakamura, R., Saga, Y. and Kopan, R. (2012). Different assemblies of Notch receptors coordinate the distribution of the major bronchial Clara, ciliated and neuroendocrine cells. *Development* **139**, 4365-4373.

Mortazavi, A., Williams, B. A., McCue, K., Schaeffer, L. and Wold, B. (2008). Mapping and quantifying mammalian transcriptomes by RNA-seq. *Nat. Met.* **5**, 621-628.

Murtaugh, L. C., Stanger, B. Z., Kwan, K. M. and Melton, D. A. (2003). Notch signaling controls multiple steps of pancreatic differentiation. *Proc. Natl. Acad. Sci. USA* **100**, 14920-14925.

Nicolas, M., Wolfer, A., Raj, K., Kummer, J. A., Mill, P., van Noort, M., Hui, C.-C., Clevers, H., Dotto, G. P. and Radtke, F. (2003). Notch1 functions as a tumor suppressor in mouse skin. *Nat. Genet.* **33**, 416-421.

Nus, M., MacGrogan, D., Martinez-Poveda, B., Benito, Y., Casanova, J. C., Fernandez-Aviles, F., Bermejo, J. and de la Pompa, J. L. (2011). Diet-induced aortic valve disease in mice haploinsufficient for the Notch pathway effector RBPJK/CSL. *Arterioscler. Thromb. Vasc. Biol.* **31**, 1580-1588.

Pan, Y., Lin, M.-H., Tian, X., Cheng, H.-T., Gridley, T., Shen, J. and Kopan, R. (2004). γ-Secretase functions through Notch signaling to maintain skin appendages but is not required for their patterning or initial morphogenesis. *Dev. Cell* **7**, 731-743.

Parr, C., Watkins, G. and Jiang, W. G. (2004). The possible correlation of Notch-1 and Notch-2 with clinical outcome and tumour clinicopathological parameters in human breast cancer. *Int. J. Mol. Med.* **14**, 779-786.

Quigley, D. A., To, M. D., Pérez-Losada, J., Pelorosso, F. G., Mao, J.-H., Nagase, H., Ginzinger, D. G. and Balmain, A. (2009). Genetic architecture of mouse skin inflammation and tumour susceptibility. *Nature* **458**, 505-508.

Radtke, F., Wilson, A., Stark, G., Bauer, M., van Meerwijk, J., MacDonald, H. R. and Aguet, M. (1999). Deficient T cell fate specification in mice with an induced inactivation of Notch1. *Immunity* **10**, 547-558.

Rangarajan, A., Talora, C., Okuyama, R., Nicolas, M., Mammucari, C., Oh, H., Aster, J. C., Krishna, S., Metzger, D., Chambon, P. et al. (2001). Notch signaling is a direct determinant of keratinocyte growth arrest and entry into differentiation. *EMBO J.* **20**, 3427-3436.

Rubio-Aliaga, I., Soewarto, D., Wagner, S., Klaften, M., Fuchs, H., Kalaydjiev, S., Busch, D. H., Klempt, M., Rathkolb, B., Wolf, E. et al. (2007). A genetic screen for modifiers of the delta1-dependent notch signaling function in the mouse. *Genetics* **175**, 1451-1463.

Rubio-Aliaga, I., Przemeck, G. K. H., Fuchs, H., Gailus-Durner, V., Adler, T., Hans, W., Horsch, M., Rathkolb, B., Rozman, J., Schrewe, A. et al. (2009). Dll1 haploinsufficiency in adult mice leads to a complex phenotype affecting metabolic and immunological processes. *PLoS ONE* **4**, e6054.

Saito, T., Chiba, S., Ichikawa, M., Kunisato, A., Asai, T., Shimizu, K., Yamaguchi, T., Yamamoto, G., Seo, S., Kumano, K. et al. (2003). Notch2 is preferentially expressed in mature B cells and indispensable for marginal zone B lineage development. *Immunity* **18**, 675-685.

Shaya, O. and Sprinzak, D. (2011). From Notch signaling to fine-grained patterning: modeling meets experiments. *Curr. Opin. Genet. Dev.* **21**, 732-739.

Simonetti, G., Carette, A., Silva, K., Wang, H., De Silva, N. S., Heise, N., Siebel, C. W., Shlomchik, M. J. and Klein, U. (2013). IRF4 controls the positioning of mature B cells in the lymphoid microenvironments by regulating NOTCH2 expression and activity. *J. Exp. Med.* **210**, 2887-2902.

Sprinzak, D., Lakhanpal, A., LeBon, L., Santat, L. A., Fontes, M. E., Anderson, G. A., Garcia-Ojalvo, J. and Elowitz, M. E. (2010). Cis interactions between Notch and Delta generate mutually exclusive signalling states. *Nature* **465**, 86-90.

Srivastava, B., Lindsley, R. C., Nikbakht, N. and Allman, D. (2005). Models for peripheral B cell development and homeostasis. *Semin. Immunol.* **17**, 175-182.

Stanley, P. and Guidos, C. J. (2009). Regulation of Notch signaling during T- and B-cell development by O-fucose glycans. *Immunol. Rev.* **230**, 201-215.

Tadeu, A. M. B. and Horsley, V. (2013). Notch signaling represses p63 expression in the developing surface ectoderm. *Development* **140**, 3777-3786.

Tagami, S., Okochi, M., Yanagida, K., Ikuta, A., Fukumori, A., Matsumoto, N., Ishizuka-Katsura, Y., Nakayama, T., Itoh, N., Jiang, J. et al. (2008). Regulation of Notch signaling by dynamic changes in the precision of S3 cleavage of Notch-1. *Mol. Cell. Biol.* **28**, 165-176.

Tanigaki, K., Han, H., Yamamoto, N., Tashiro, K., Ikegawa, M., Kuroda, K., Suzuki, A., Nakano, T. and Honjo, T. (2002). Notch-RBP-J signaling is involved in cell fate determination of marginal zone B cells. *Nat. Immunol.* **3**, 443-450.

Theodoris, C. V., Li, M., White, M. P., Liu, L., He, D., Pollard, K. S., Bruneau, B. G. and Srivastava, D. (2015). Human disease modeling reveals integrated transcriptional and epigenetic mechanisms of NOTCH1 haploinsufficiency. *Cell* **160**, 1072-1086.

van Tetering, G., van Diest, P., Verlaan, I., van der Wall, E., Kopan, R. and Vooijs, M. (2009). The metalloprotease ADAM10 is required for Notch1 Site 2 cleavage. *J. Biol. Chem.* **284**, 31018-31027.

Varadkar, P., Kraman, M., Despres, D., Ma, G., Lozier, J. and McCright, B. (2008). Notch2 is required for the proliferation of cardiac neural crest-derived smooth muscle cells. *Dev. Dyn.* **237**, 1144-1152.

Varnum-Finney, B., Halasz, L. M., Sun, M., Gridley, T., Radtke, F. and Bernstein, I. D. (2011). Notch2 governs the rate of generation of mouse long- and short-term repopulating stem cells. *J. Clin. Invest.* **121**, 1207-1216.

Winston, J. B., Erlich, J. M., Green, C. A., Aluko, A., Kaiser, K. A., Takematsu, M., Barlow, R. S., Sureka, A. O., LaPage, M. J., Janss, L. L. et al. (2010). Heterogeneity of genetic modifiers ensures normal cardiac development. *Circulation* **121**, 1313-1321.

Witt, C. M., Won, W.-J., Hurez, V. and Klug, C. A. (2003). Notch2 haploinsufficiency results in diminished B1 B cells and a severe reduction in marginal zone B cells. *J. Immunol.* **171**, 2783-2788.

Yang, X., Klein, R., Tian, X., Cheng, H.-T., Kopan, R. and Shen, J. (2004). Notch activation induces apoptosis in neural progenitor cells through a p53-dependent pathway. *Dev. Biol.* **269**, 81-94.

Zhang, N., Martin, G. V., Kelley, M. W. and Gridley, T. (2000). A mutation in the Lunatic fringe gene suppresses the effects of a Jagged2 mutation on inner hair cell development in the cochlea. *Curr. Biol.* **10**, 659-662.

Zheng, Y., de la Cruz, C. C., Sayles, L. C., Alleyne-Chin, C., Vaka, D., Knaak, T. D., Bigos, M., Xu, Y., Hoang, C. D., Shrager, J. B. et al. (2013). A rare population of CD24(+)ITGB4(+)Notch(hi) cells drives tumor propagation in NSCLC and requires Notch3 for self-renewal. *Cancer Cell* **24**, 59-74.

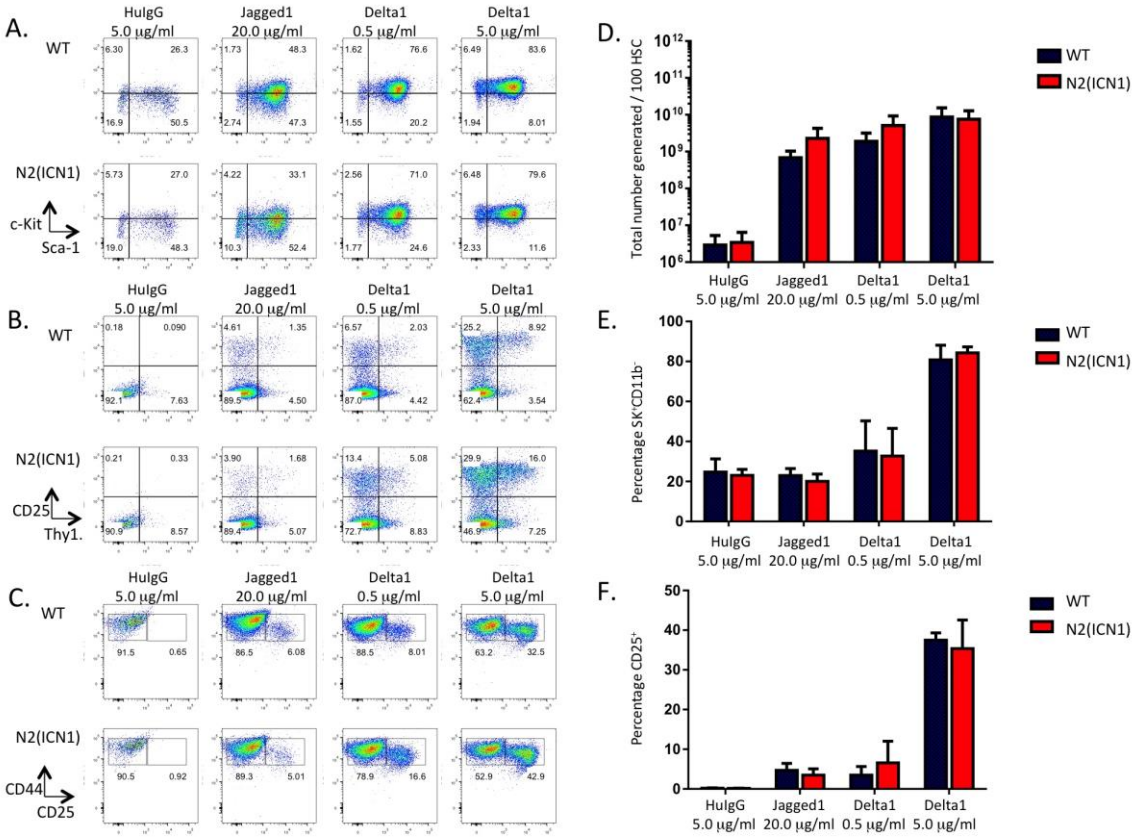

Fig. S1. **Notch1 ICD swapped into Notch2 locus functionally replaces Notch2 ICD during Notch2-dependent ex vivo culture with Notch ligands Delta and Jagged. (**A-C) Representative dot plots after 14 day bone marrow (BM) HSC culture on plastic coated with either different densities of immobilized Delta1, Jagged1 (extracellular domain Delta1 or Jagged1 fused to Fc domain of Human IgG) or control Human IgG. Boxes in C indicate DN1 ($CD44^+CD25^-$) and DN2 ($CD44^+CD25^+$) subpopulations. (D) Total number of cells, (E) percent Sca^+ Kit^+ $CD11b^-$ cells, and (F) percent $CD25^+$ cells generated in cultures initiated with 100 FACS isolated HSC after 14 days of culture. Data represent mean +/- SEM from 4 independent experiments. p values were determined with 2-tailed paired Student's t test. Numbers within dot plots denote percentage of events within the respective gates.

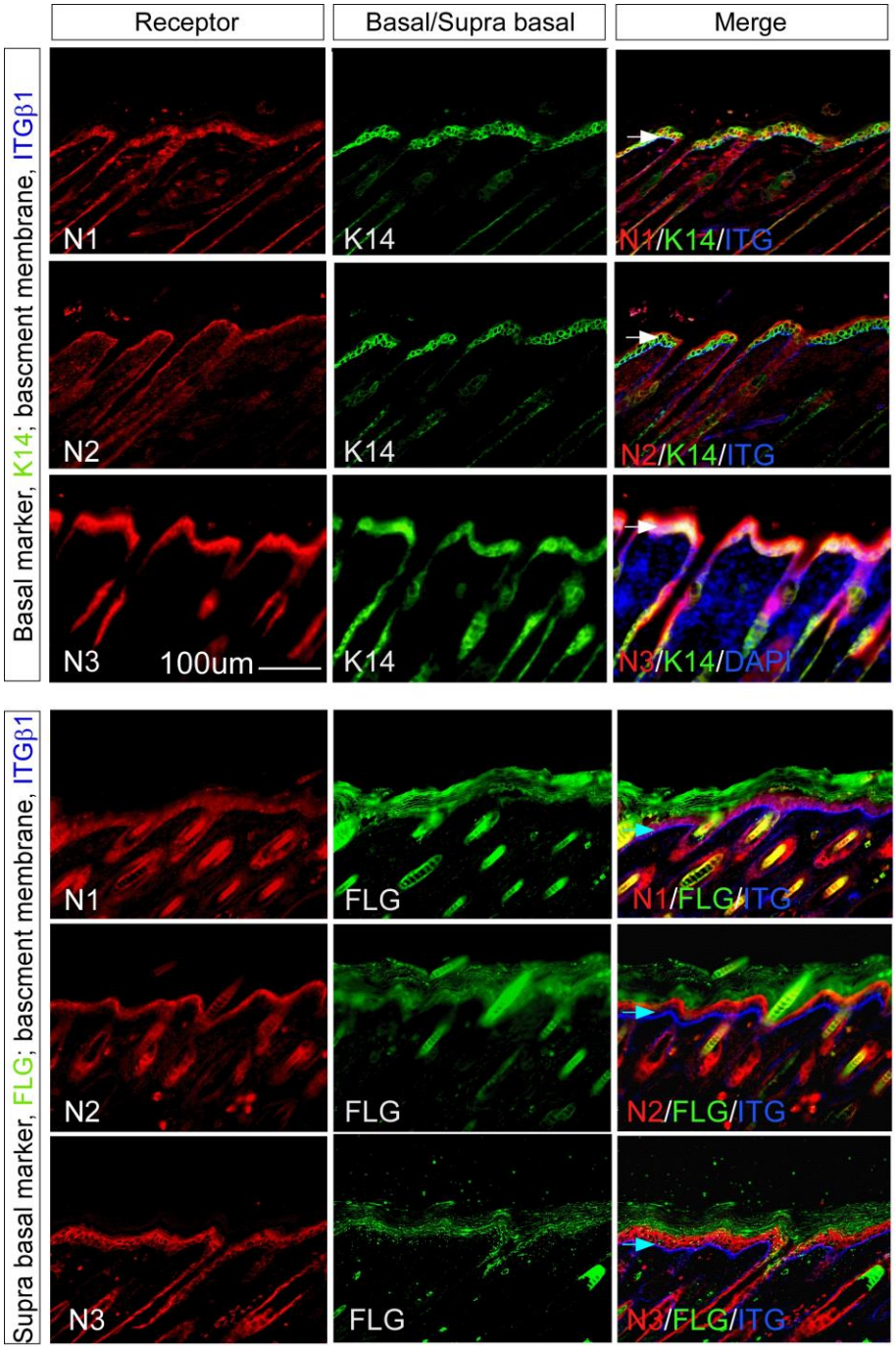

Fig. S2. Detailed analysis of the expression pattern of Notch1, Notch2 and Notch3 in the epidermis of wild type postnatal day 9 (P9) pups. Whereas Notch1 and Notch3 are expressed in both basal (marked by K14 antibody staining) and supra basal (marked by filagrin (FLG) antibody staining) cell layers, Notch2 is only expressed in supra basal cells. Arrows in the merged images indicate the basal cell layer, whose basal membrane is marked by the expression of β1 integrin (ITGβ1).

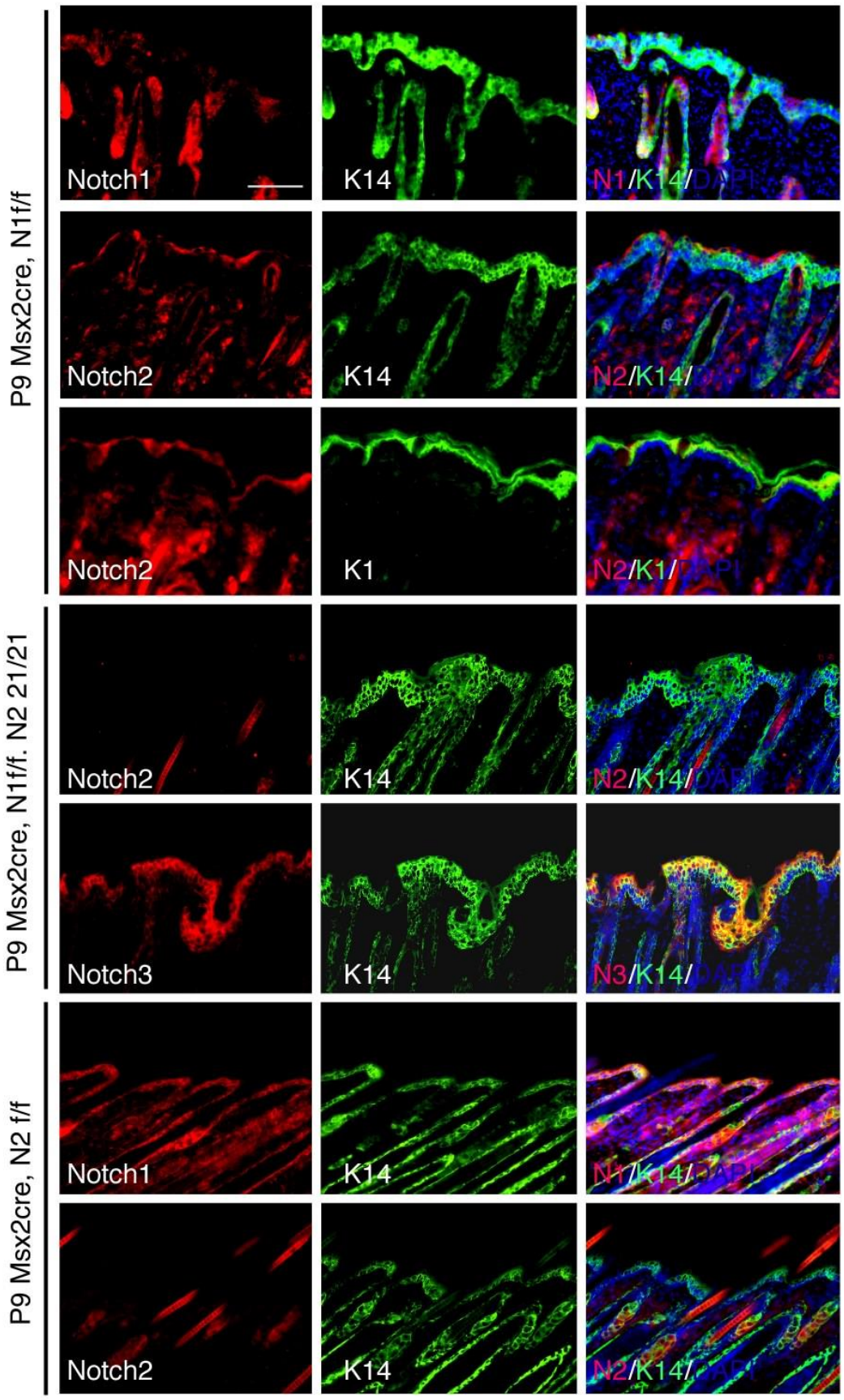
P9 Msx2cre, N1f/f
Notch1
K14
N1/K14/DAPI
Notch2
K14
N2/K14/
Notch2
K1
N2/K1/
P9 Msx2cre, N1f/f. N2 21/21
Notch2
K14
N2/K14/
Notch3
K14
N3/K14/
P9 Msx2cre, N2 f/f
Notch1
K14
N1/K14/
Notch2
K14
N2/K14/

Fig. S3. The expression of Notch1, Notch2 and Notch3 in various mutant skin at P9. Basal cells are marked with K14 and supra basal cells with K1. In the skin of Msx2cre, $N1^{f/f}$ pups, complete loss of Notch1 is observed in mutant area marked by hyper-proliferation of basal cells. N2ICD is replaced by N1ICD in the skin of Msx2Cre, $N1^{f/f}$; $N2^{21/21}$ pups, but basal cell hyper proliferation is still evident. In the skin of Msx2Cre, $N2^{f/f}$, the complete loss of Notch2 does not result in basal cell hyper-proliferation.

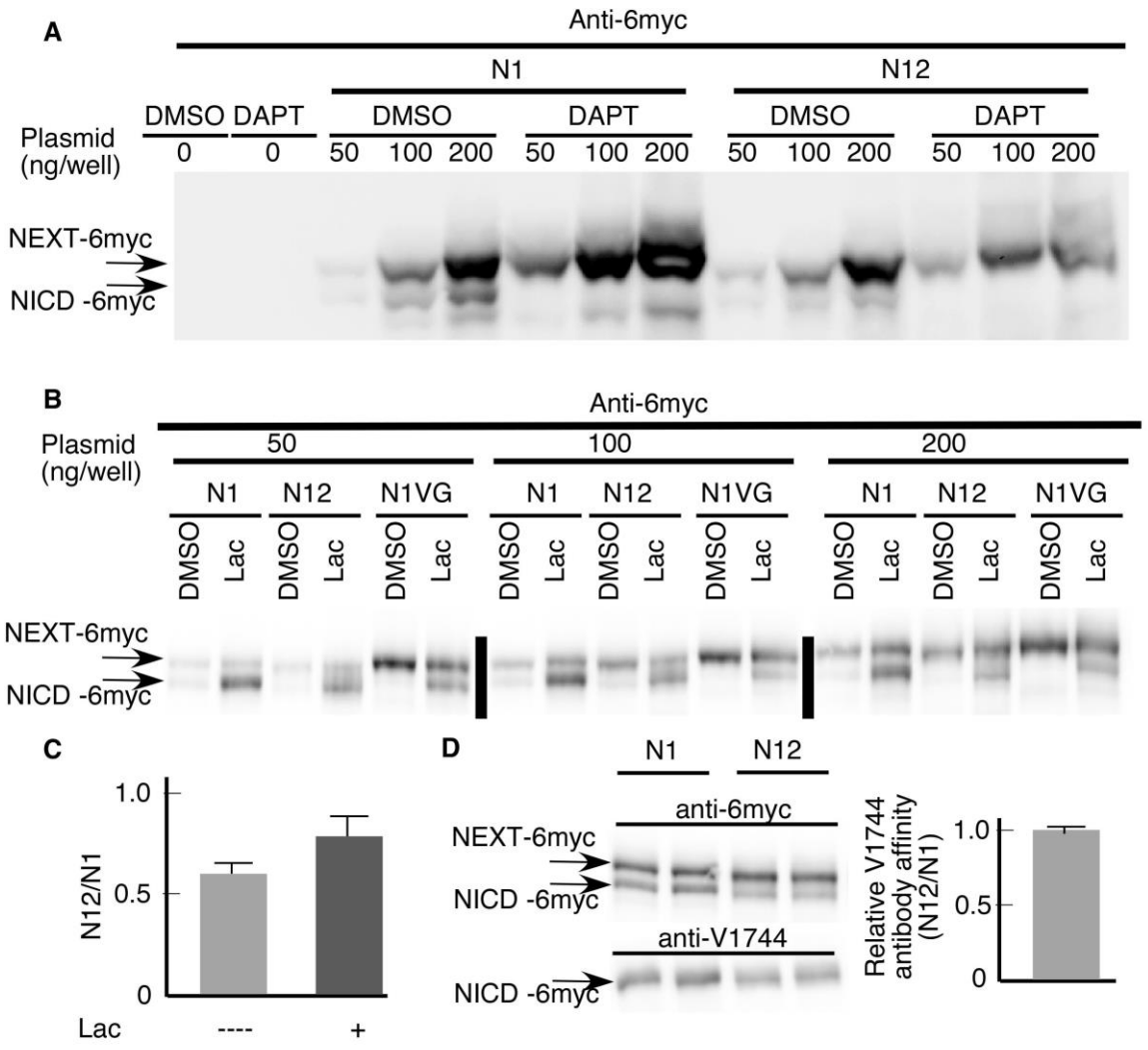

Fig. S4. Analysis of cleavage efficiency of the N12 protein and the stability of N12ICD in cultured HEK293 cells. (A-B) HEK293 cells were transfected with various amount of plasmid expressing a c-terminal tagged proteins; pCS2ΔE-Notch1-6xmyc (N1), pCS2ΔE-Notch12-6xmyc (N12) (A, B), or pCS2ΔE-Notch1 V1744G-6xmyc (N1VG) plasmid (B). (A) Uncleaved fragment (NEXT-6myc) and γ-secretase cleaved fragment (NICD-6myc) were detected with anti-Myc antibody. In the presence of γ-secretase inhibitor DAPT, the production of the cleaved fragment is dramatically reduced whereas the uncleaved fragment increases, validating the identity of the NICD. (B) The presence of proteasome inhibitor Lactacystin (Lac) dramatically increased the amount of the NICD. (C) Quantification of relative NICD level shows that in the absence of Lac, the cleaved N1ICD level in cells transfected with pCS2ΔE-

Notch12-6xmyc (N12) is about 50% of that of pCS2ΔE-Notch1-6xmyc (N1). The presence of Lac increases this ratio to ~75%, suggesting that both the stability of the cleaved ICD from N12 and the cleavage efficiency of the N12 chimeric protein are reduced relative to the wild type N1 locus in cultured 293 cells. (D) To examine whether the binding affinity of anti-V1744 antibody is affected by intracellular amino acids, the same lysates from cells transfected with pCS2ΔE-Notch1-6xmyc (N1) and pCS2ΔE-Notch12-6xmyc (N12) were probed with anti-Myc tag and anti-V1744 antibodies, respectively, and the relative signal intensity was calculated. The results show that the affinity of anti-V1744 antibody was unaffected by the intracellular composition.

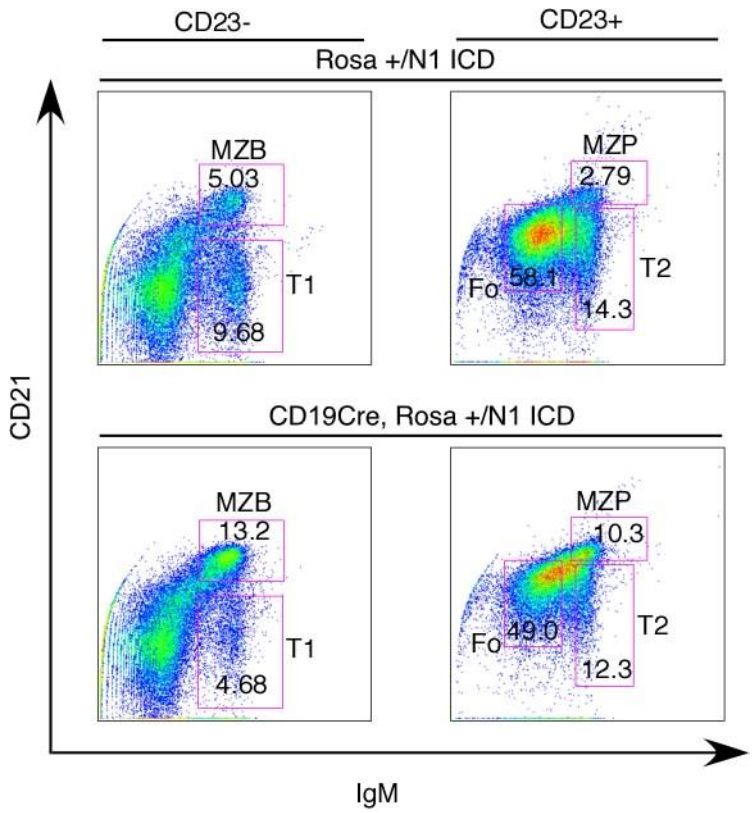

Fig. S5. Rosa^{Notch}; CD19-Cre mice released N1ICD in the B cell lineage and could efficiently drive the differentiation of MZP and MZB cells when overexpressed.